



Title	Incomplete Elongation of Ultra-long-chain Polyunsaturated Acyl-CoAs by the Fatty Acid Elongase ELOVL4 in Spinocerebellar Ataxia Type 34
Author(s)	Tamura, Yuka; Sassa, Takayuki; Nishizawa, Takumi; Kihara, Akio
Citation	Molecular and cellular biology, 43(2), 85-101 https://doi.org/10.1080/10985549.2023.2169563
Issue Date	2023-02-07
Doc URL	http://hdl.handle.net/2115/91300
Rights	This is an Accepted Manuscript of an article published by Taylor & Francis in Molecular and Cellular Biology on 07 Feb. 2023, available at: http://www.tandfonline.com/10.1080/10985549.2023.2169563 .
Type	article (author version)
File Information	MCB00392-22R1_Merged_PDF.pdf



[Instructions for use](#)

1 **Incomplete elongation of ultra-long-chain polyunsaturated acyl-CoAs by**
2 **the fatty acid elongase ELOVL4 in spinocerebellar ataxia type 34**

3

4 Yuka Tamura,^a Takayuki Sassa,^a Takumi Nishizawa,^a Akio Kihara^a

5 ^aLaboratory of Biochemistry, Faculty of Pharmaceutical Sciences, Hokkaido University,

6 Sapporo, Japan

7

8 Running title: Pathogenesis of spinocerebellar ataxia type 34

9

10 Address correspondence to Takayuki Sassa (tasasa@pharm.hokudai.ac.jp) and Akio Kihara
11 (kihara@pharm.hokudai.ac.jp)

12

13 **ABSTRACT**

14 Spinocerebellar ataxias (SCAs) are autosomal dominant diseases characterized by
15 cerebellar atrophy and ataxia. The SCA subtype SCA34 is caused by specific mutations in
16 the gene *ELOVL4*, which encodes a fatty acid (FA) elongase that synthesizes
17 ultra-long-chain (ULC; \geq C26) FAs. However, the pathogenesis and molecular mechanism
18 that confers dominant inheritance remains unknown. Here, a cell-based assay demonstrated
19 that each of the five known SCA34 mutants produced shorter ULC polyunsaturated
20 FA-containing phosphatidylcholines (ULC-PCs) than wild-type protein, in the following
21 order of severity: Q180P and T233M > W246G > I171T and L168F. Next, we generated
22 knock-in mouse embryonic stem cells that contained heterozygous Q180P, heterozygous
23 W246G, or homozygous W246G mutations. Neuronal differentiation-dependent production
24 of ULC-PCs was reduced in heterozygous Q180P and homozygous W246G cells relative to
25 control cells, and we observed shortening of the FA moiety in all mutant cells. This FA
26 shortening was consistent with our prediction that amino acid residues substituted by
27 SCA34 mutations are located in the transmembrane helices that interact with the ω -end
28 region of the FA moiety of the substrate acyl-CoA. Hence, reduced levels and shortening of
29 ULC-PCs in neurons may cause SCA34, and incomplete elongation of ULC
30 polyunsaturated acyl-CoAs by mutated *ELOVL4* may induce dominant inheritance.

31

32 **KEYWORDS**

33 ELOVL4, spinocerebellar ataxia, fatty acid, neuron, polyunsaturated fatty acid

34

35 INTRODUCTION

36 The spinocerebellar ataxias (SCAs) are a group of cerebellar ataxias that are inherited in an
37 autosomal dominant manner and characterized by cerebellar atrophy and ataxia (1, 2).
38 Currently, there exist 49 SCA subtypes; for most of them, causative genes have been
39 identified (1, 3). Each causative gene exhibits a particular type of mutation, such as
40 expansion of CAG repeats encoding the polyglutamine tract, expansion of non-coding
41 repeats, missense mutations, or frameshift mutations (1). It is thought that these mutations
42 have gain-of-function, dominant negative, or loss-of-function (leading to
43 haploinsufficiency) effects. They cause various cellular abnormalities, including
44 transcriptional dysregulation, RNA toxicity, ion channel dysfunction, and mitochondrial
45 dysfunction. One type of SCA, namely SCA34, is caused by mutations in the fatty acid
46 (FA) elongase *ELOVL4*.

47 *ELOVL4* is one of the seven FA elongases (*ELOVL1–7*) that exist in mammals (4, 5).
48 FAs are classified according to their chain-length; they can be categorized as long-chain
49 FAs (C11–C20) or very-long-chain (VLC) FAs (\geq C21). VLCFAs with C26 or more are
50 termed ultra-long-chain (ULC) FAs (4, 5). FAs are also classified according to their degree
51 of unsaturation and are categorized as saturated FAs (SFAs), monounsaturated FAs
52 (MUFAs), or polyunsaturated FAs (PUFAs). The long-chain FAs synthesized by FA
53 synthase in the cytosol or incorporated from dietary sources are subject to elongation via
54 the FA elongation cycle, which consists of four sequential reactions and takes place in the

55 endoplasmic reticulum (ER). ELOVLs catalyze the rate-limiting reaction: condensation of
56 an acyl-CoA—the activated form of FA—with a malonyl-CoA (6). Each ELOVL isozyme
57 exhibits characteristic substrate specificity toward acyl-CoAs with different chain-lengths
58 and/or degrees of unsaturation (7). Of the ELOVLs, only ELOVL4 is responsible for
59 generating ULCFAs, regardless of the saturation/unsaturation type (SFAs, MUFAs, and
60 PUFAs) (4, 5, 7). Thus far, five missense mutations—L168F
61 [NM_022726.4(ELOVL4):c.504G>C (p.Leu168Phe), rs587777598], I171T
62 [NM_022726.4(ELOVL4):c.512T>C (p.Ile171Thr), rs1554162301], Q180P
63 [NM_022726.4(ELOVL4):c.539A>C (p.Gln180Pro)], T233M
64 [NM_022726.4(ELOVL4):c.698C>T (p.Thr233Met), rs1554162016], and W246G
65 [NM_022726.4(ELOVL4):c.736T>G (p.Trp246Gly), rs1131692036]—have been identified
66 in *ELOVL4* as mutations that cause SCA34. Gait ataxia, nystagmus, and dysarthria have
67 been reported as common neurological abnormalities in patients with these mutations (8–
68 17). Skin erythrokeratoderma was also observed in patients carrying one of the mutations
69 L168F, Q180P, and T233M (11, 12, 16), while retinitis pigmentosa was observed in a
70 subset of patients harboring the I171T mutation (17). The age of onset differs among the
71 mutations: 10–20 years for Q180P; 10–50 years for T233M and W246G; 30–50 years for
72 I171T; and 30–70 years for L168F. Recently, knock-in (KI) rats harboring the W246G
73 mutation have been generated (18). Assessment using the rotarod performance test revealed
74 that heterozygous and homozygous W246G KI rats exhibited impaired motor function

75 without apparent histological abnormalities, while homozygous W246G KI rats exhibited
76 impaired synaptic plasticity in parallel and climbing fibers in the cerebellum (18). However,
77 the effects of the SCA34 mutations on ELOVL4 enzymatic activity have not been
78 examined, and the mechanism underlying the pathogenesis and autosomal dominant
79 inheritance mode of SCA34 remains unclear.

80 Distinct sets of mutations in the *ELOVL4* gene are associated with two other hereditary
81 diseases: Stargardt disease 3 (STGD3) and ISQMR (ichthyosis, spastic quadriplegia, and
82 mental retardation) (19). STGD3 is a type of juvenile macular dystrophy without other
83 neurological or skin symptoms that is inherited in an autosomal dominant manner. Three
84 *ELOVL4* mutations (frameshift mutations N264LfsX10 and N264TfsX9 and the nonsense
85 mutation Y270X) have been identified in STGD3 (20–22). It has been predicted that these
86 mutations produce mutant ELOVL4 proteins lacking the C-terminal of approximately 50
87 residues, including the ER retention motif. Several studies have demonstrated that these
88 mutant proteins exert dominant negative effects on wild-type (WT) ELOVL4 protein in the
89 retinal photoreceptor cells (23–26). Alternatively, the mutant proteins can be abnormally
90 transported to the outer segment of photoreceptors and phagocytosed by the retinal pigment
91 epithelium, where they cause non-cell-autonomous toxic effects (27, 28). ISQMR is an
92 autosomal recessive neurodevelopmental and cutaneous disorder characterized by skin
93 ichthyosis (scaly and dry skin), spastic quadriplegia, seizures, and intellectual disability.
94 Six *ELOVL4* mutations have been identified in ISQMR (nonsense mutations Y26X, R70X,

95 and R216X; frameshift mutations I146YfsX29 and I230MfsX22; and the missense
96 mutation C163R) (29–31). R70X and C163R were found together in one compound
97 heterozygous patient, while the other mutations have been found in homozygous patients.
98 Except for C163R, all mutations produce a truncated ELOVL4 protein lacking more
99 C-terminal residues than STGD3 mutant proteins. The C163R mutation causes substitution
100 of the amino acid located near the catalytically essential histidine-motif (residues 158–162).
101 These findings, together with the recessive mode of inheritance, suggest that the ISQMR
102 mutations have loss-of-function effects. Since heterozygous carriers of ISQMR do not
103 exhibit symptoms (29–31), SCA34 is not caused by the simple haploinsufficiency of
104 *ELOVL4*. Other mechanisms may be responsible for rendering the disease dominant.

105 *ELOVL4* is abundantly expressed in the retina, skin, testes, meibomian glands, and
106 brain (mainly in neurons) (32). In the retina, phosphatidylcholines (PCs) containing ULC
107 PUFAs (ULC-PCs) are present and important for visual function (33, 34). In the skin, ULC
108 SFAs/MUFAs are essential for the formation of the epidermal permeability barrier, as they
109 are components of ω -*O*-acylceramides, which are specialized barrier lipids (4, 35, 36). In
110 the testes, ULC PUFAs are used to create glycosphingolipids and sphingomyelins and are
111 essential for spermatogenesis (37). In the meibomian glands, ULC SFAs/MUFAs are used
112 to create cholesteryl esters, wax monoesters/diesters, and (*O*-acyl)- ω -hydroxy FAs, which
113 are secreted as the constituents of tear film lipids and play an important role in preventing
114 dry eye disease (38–42). In the brain, ULC PUFAs are predominantly present in PCs, in

115 which ULC PUFAs with four to six double bonds occupy the *sn*-1 position (43, 44).
116 However, the functions of ULC-PCs in the nervous system and their relationships with
117 SCA34 and ISQMR remain unexplored.

118 The aim of this study was to elucidate the pathogenesis of SCA34 and the molecular
119 mechanism that causes its dominant heritability. For this purpose, we deduced the positions
120 of substituted amino acid residues in ELOVL4 protein based on the recently resolved
121 crystal structure of ELOVL7 (45). We then examined the intracellular localization of
122 mutant proteins and measured the FA elongation activity of the mutant proteins in a
123 cell-based overexpression system. Furthermore, we generated mouse embryonic stem (ES)
124 cells carrying the Q180P or W246G mutation and measured the levels and FA composition
125 of ULC-PCs in them. Through these analyses, we obtained clues about the pathogenesis of
126 SCA34 and the molecular mechanism causing its dominant mode of inheritance.

127 **RESULTS**

128 **SCA34 mutations cause amino acid substitutions in the regions involved in the**
129 **binding of the FA moiety of acyl-CoA in ELOVL4 protein.** It has been established that
130 five *ELOVL4* missense mutations cause SCA34 (Fig. 1). However, the position of these
131 amino acid residues in the 3D structure of the ELOVL4 protein remains unclear. In this
132 study, we mapped the amino acid residues of ELOVL4 substituted in SCA34 onto the
133 recently revealed crystal structure of the human ELOVL7 protein (PDB: 6Y7F) (45), which
134 is one of the seven isozymes of the ELOVL family. The amino acid residues of ELOVL4
135 mutated in SCA34 were L168F, I171T, Q180P, T233M, and W246G, and correspond to
136 residues T157, F160, L169, I222, and F238 from ELOVL7, respectively (Fig. 1). These
137 five residues are not conserved but rather diverged among ELOVL isozymes. In the crystal
138 structure of ELOVL7, these amino acid residues were mapped in the transmembrane helix
139 (TMH) 4 (L168F and I171T), TMH5 (Q180P), TMH6 (T233M), and TMH7 (W246G) (Fig.
140 2). These residues were not located close to the catalytic site consisting of a histidine box,
141 but rather located at the ω -end region of the FA moiety of the bound acyl-CoA analog (Fig.
142 2). Thus, the amino acid residues of ELOVL4 substituted in SCA34 constitute the substrate
143 binding site and may participate in the acquisition of substrate specificity in terms of the
144 FA chain length of acyl-CoAs.

145

146 **SCA34 mutant proteins are localized in the ER.** Although WT ELOVL4 is localized in
147 the ER, it has been reported that STGD3 mutations affect its subcellular localization (23,
148 27). On the other hand, the effect of SCA34 mutations on subcellular localization has not
149 been investigated. To address this, five SCA34 mutants and WT protein as a control were
150 transiently expressed in HeLa cells as 3×FLAG-tagged proteins. Subsequently, their
151 subcellular localization was examined using indirect immunofluorescence microscopy.
152 Consistent with a previous report (7), WT ELOVL4 protein was localized in the ER, as
153 demonstrated by its colocalization with the ER marker calnexin (Fig. 3). All five SCA34
154 mutant proteins were also localized in the ER, indicating that the SCA34 mutations do not
155 affect intracellular localization.

156

157 **SCA34 mutants produce shorter ULC lipids than WT ELOVL4.** To investigate the
158 effect of SCA34 mutations on the ULCFA-producing activity of ELOVL4, we
159 overproduced 3×FLAG-tagged WT ELOVL4 or each of the SCA34 mutants in HEK 293T
160 cells, extracted the lipids from these cells, and measured the quantities of ceramides and
161 PCs via liquid chromatography (LC)–tandem mass spectrometry (MS/MS). As a control,
162 we also overproduced R216X ISQMR mutant, which lacks a C-terminus (one-third of the
163 protein) and therefore likely has no enzymatic activity. Since ceramides can contain
164 saturated, monounsaturated, or polyunsaturated ULCFA, measurement of ceramides is
165 useful for monitoring the FA elongation activity of ELOVL4 towards each type of

166 acyl-CoA. To produce ULC polyunsaturated ceramides (Fig. 4A), HA-tagged ELOVL2
167 [synthesizes C24 PUFAs (7), the substrates for the synthesis of ULC PUFAs (Fig. 4B)] and
168 3×FLAG-tagged CERS3 [synthesizes ULC ceramides using ULC acyl-CoAs as substrates
169 (46, 47)] were co-overproduced with 3×FLAG-ELOVL4. In the immunoblot analysis, WT
170 ELOVL4 protein was detected as two bands, an upper glycosylated form and a lower
171 non-glycosylated form (Fig. 4C) (7). All five SCA34 mutant proteins were also detected as
172 two bands, with expression levels comparable to that of WT proteins. Two bands of the
173 R216X ISQMR mutant protein were observed (24 and 27 kDa), consistent with the large
174 C-terminus truncation. For the LC–MS/MS analysis, the levels of ceramides produced by
175 each ELOVL4 mutant were shown as a ratio to those produced by WT ELOVL4 and
176 displayed as a heat map (Fig. 4D). In cells expressing the R216X ISQMR mutant, the
177 ceramide composition was similar to that noted in cells transfected with an empty vector.
178 This composition included reduced levels of \geq C28 saturated/monounsaturated ceramides
179 and \geq C32 polyunsaturated ceramides, with concomitant increases in the shorter species
180 compared with WT ELOVL4-expressing cells (Fig. 4D and E; E indicates C32:6 and C38:6
181 ceramide levels as representatives). These results demonstrated that as expected, the R216X
182 mutant does not have activity. In cells expressing the SCA34 mutants, the levels of
183 numerous ceramide species containing \geq C34 ULC PUFA were decreased, accompanied by
184 increases in the levels of \leq C32 polyunsaturated ceramides (Fig. 4D). An exception to this
185 finding was the L168F mutant; its expression resulted in decreases in most \geq C30 species,

186 except C38:4 and C38:5. The chain-length-shortening effect of the SCA mutations was
187 strongest for the Q180P and T233M mutants, followed by W246G, I171T, and L168F.
188 Shortening was also observed for saturated and monounsaturated ceramides by many of the
189 SCA mutants. Nevertheless, shortening was not observed for saturated ceramides by the
190 Q180P mutant and for monounsaturated ceramides by the L168F and I171T mutants.

191 Next, to measure ULC-PCs (Fig. 4A), which are present in neurons,
192 3×FLAG-ELOVL4 WT or each of the SCA34 mutants were overexpressed together with
193 HA-ELOVL2 in HEK 293T cells. The expression levels of these proteins were confirmed
194 by immunoblot analysis (Fig. 4F). Lipids were extracted, and ULC-PCs were measured via
195 LC-MS/MS. Each PC species was expressed according to the sum of its chain length and
196 the number of double bonds in its two constituent FAs. Again, PC composition in cells
197 expressing the R216X ISQMR mutant was similar to that recorded in vector-transfected
198 cells (Fig. 4G). Numerous \geq C50 ULC-PC species were reduced and \leq C48 species were
199 increased compared with those measured in WT ELOVL4-expressing cells. In the cells
200 expressing the SCA34 mutants, the levels of PCs with \geq C52 decreased, whereas levels of
201 PCs with \leq C50 increased in most cases. The heatmap pattern of ULC-PCs for each SCA34
202 mutant was similar to that of polyunsaturated ceramides (Fig. 4D and G), confirming the
203 above observed activity of SCA34 mutants towards ULC polyunsaturated acyl-CoAs.
204 Comparison of the two heatmaps suggested, for example, that the C32:6 ceramide species
205 corresponds to the C50:7 PC species. Therefore, the C50:7 PC species mainly consists of

206 C32:6 ULC PUFA and C18:1 FA (oleic acid) in the *sn*-1 and *sn*-2 positions, respectively
207 (Fig. 4A). Such PC species have been reported in human and rat brains (43, 44). These
208 results indicate that the SCA34 mutations cause incomplete elongation of ULC
209 polyunsaturated acyl-CoAs and shortening of the ULC PUFA-containing lipids.

210

211 **Neuronal differentiation increases ULC-PC levels.** In the brain, *ELOVL4* is
212 predominantly expressed in neurons (32), and ULC PUFAs synthesized by ELOVL4
213 mainly exist in PCs (43, 44). In the present study, we utilized neurons differentiated from
214 ES cells as model neurons. Mouse ES cells were subjected to differentiation into neurons
215 via the formation of embryoid bodies, treatment with retinoic acids, and growth in neuronal
216 differentiation medium (48). This protocol efficiently induced the differentiation of ES cells
217 into neurons, as demonstrated by their cell morphology and the expression of the neuronal
218 marker class III β -tubulin (Fig. 5A). To confirm *Elovl4* mRNA expression and ULC-PC
219 production in these cells, total RNA and lipids were extracted, and the levels of *Elovl4*
220 mRNAs and ULC-PCs were examined by quantitative RT-PCR and LC-MS/MS,
221 respectively. Both *Elovl4* mRNA and ULC-PC levels increased as the cells differentiated
222 (Fig. 5B and C). Thus, neurons differentiated from ES cells are useful for the evaluation of
223 ELOVL4 activity.

224

225 **Neurons with SCA34 mutations produce shortened ULC-PCs.** To clarify the effects of
226 SCA34 mutations on the levels and composition of ULC-PCs, the Q180P and W246G
227 mutations were each introduced into the *Elovl4* gene in mouse ES cells using
228 single-stranded oligodeoxynucleotide-mediated KI with a CRISPR/Cas9 system (49).
229 These mutations were selected as severe (Q180P) and moderate (W246G) examples in
230 terms of the age of disease onset (12, 50) and their shortening effect on ULC-lipids (Fig. 4).
231 A heterozygous KI clone, which mimics the dominant form of inheritance in SCA34, was
232 obtained for each mutation. A homozygous KI clone, which likely exhibits more changes
233 than the corresponding heterozygous KI clone, was obtained for the W246G mutation (Fig.
234 6A). These KI and control ES cells were differentiated into neurons, and the lipids prepared
235 after 1 and 5 days of differentiation were subjected to quantification of ULC-PCs by LC–
236 MS/MS. After 1 day of differentiation, the total levels of ULC-PCs in W246G homozygous
237 KI cells were reduced to 42% of those noted in control cells (Fig. 6B). On the other hand,
238 heterozygous Q180P and W246G cells exhibited reduction tendencies, which were not
239 statistically significant. The proportion of \geq C52 ULC-PCs, which mainly consists of \geq C34
240 ULC PUFAs, among the total ULC-PCs was lower in Q180P heterozygous and W246G
241 homozygous KI cells than in control cells. These findings were suggestive of ULC PUFA
242 shortening. The proportion of \geq C52 ULC-PCs in W246G heterozygous KI cells was
243 slightly higher than that recorded in control cells at this early stage of differentiation. After
244 5 days of differentiation, total ULC-PC levels had reduced significantly in W246G

245 homozygous KI cells (reduction to 43%) and Q180P heterozygous KI cells (reduction to
246 44%). On the other hand, W246G heterozygous KI cells exhibited a reduction tendency,
247 which was not statistically significant. The proportions of \geq C52 ULC-PCs in all three KI
248 cells were lower than that measured in control cells. The observed reduction and shortening
249 of ULC-PCs in KI cells were not due to the reduced expression of *Elovl* genes involved in
250 the synthesis of ULC PUFA or defective differentiation into neurons. This conclusion is
251 based on a lack of reduced expression levels of *Elovl4*, *Elovl2*, *Elovl5*, and the neuronal
252 differentiation marker *Tubb3* (encodes class III β -tubulin) in the KI cells after 5 days of
253 differentiation (Fig. 6C). Rather, increases in the levels of *Elovl4* and *Tubb3* in Q180P
254 heterozygous KI cells and in those of *Elovl2* in W246G heterozygous KI cells were
255 observed. These results indicate that polyunsaturated acyl-CoA elongation is incomplete in
256 neurons possessing SCA34 mutations and suggest that decreases and/or shortening of
257 ULC-PCs are associated with the pathogenesis of SCA34.
258

259 **DISCUSSION**

260 Five *ELOVL4* missense mutations have been identified in patients with SCA34 (12, 15, 50).
261 In the present study, all five amino acid residues substituted in SCA34 were mapped to
262 TMHs that interact with the ω -end region of the FA moiety of the substrate acyl-CoA based
263 on the 3D structure of ELOVL7 (Fig. 2) (45). WT ELOVL4 protein exhibits activity for the
264 elongation of C24 or C26 acyl-CoA to become C36 or C38 (Fig. 4) (4, 51). This indicates
265 that its substrate-binding pocket has sufficient space to accommodate a C36 or C38 ULC
266 acyl-CoA. Each of the SCA34 mutations may alter the pocket structure so that it can only
267 accommodate shorter ULC acyl-CoAs, leading to incomplete elongation of acyl-CoAs (in
268 the case of polyunsaturated acyl-CoAs, up to C32; Figs 4 and 6). The effects of the Q180P,
269 T233M, and W246G mutations on the elongation of polyunsaturated ULC acyl-CoA were
270 greater than those of L168F and I171T (Fig. 4). There was thus a correlation between the
271 degree of ULC-PC shortening and the age of disease onset (see Introduction) (12, 50). The
272 Q180P mutation affected the elongation of polyunsaturated and monounsaturated ULC
273 acyl-CoAs, but did not affect saturated ULC acyl-CoAs (Fig. 4). The Gln180 residue is
274 present in TMH5, so its α -helix structure is likely disrupted by the Gln-to-Pro substitution,
275 leading to a structural change in the substrate-binding pocket that alters the substrate
276 specificity depending on the saturation/unsaturation status.

277 In this study, we found that the levels of \geq C52 PCs were lower in Q180P and W246G
278 heterozygous KI neurons compared with control neurons (Fig. 6B). In addition, Q180P

279 heterozygous KI neurons showed a decrease in total ULC-PC levels. These results suggest
280 that the shortening of ULC PUFAs and reduction in ULC-PCs in neurons are involved in
281 the pathogenesis of SCA34. The shortening of ULC PUFAs is particularly important, since
282 it was observed in all five SCA34 mutations (Fig. 4). The \geq C52 ULC-PCs may play an
283 important role in neuronal functions; hence, they cannot be replaced by shorter ULC-PCs.
284 Although the presence of ULC-PCs has long been recognized (33, 34), their function in
285 neurons remains unknown. Neurons like the Purkinje cells in the cerebellum have very
286 complex structures, including highly branched neurites and synapses. Given the special
287 structure of ULC-PCs, with a ULC PUFA in the *sn*-1 position, they may be enriched in
288 membranes that make up complex structures like neurites and synapses, and the shortening
289 of ULC PUFAs may impair their function in these structures.

290 In this study, we also analyzed the R216X mutation, one of the causative mutations in
291 recessively inherited ISQMR. In a cell-based assay, the R216X mutant did not exhibit
292 activity for the production of ULC ceramides or ULC-PCs (Fig. 4). Thus, the R216X
293 mutation has a loss-of-function effect, which is consistent with the recessive inheritance
294 mode of ISQMR. Since the R216X mutant lacks TMH6 and subsequently the C-terminal
295 region, it cannot form the substrate-binding pocket for acyl-CoAs.

296 Although the R216X ISQMR mutant did not exhibit activity, SCA34 mutants had
297 residual activity. The neurological symptoms of ISQMR are severe and become evident
298 within the first few months to 1 year after birth (29). In contrast, the symptoms of SCA34

299 are milder than those of ISQMR, with the onset of disease mostly observed in middle age
300 (12, 50). Thus, SCA34 pathology may develop due to long-term decreases and/or changes
301 in the quality (shortening) of ULC-PCs in neurons in the cerebellum, which may be more
302 susceptible than other brain regions.

303 We speculate that the cause of the dominant inheritance mode of SCA34 is the
304 substitution of highly functional \geq C52 ULC-PCs (ULCFA moiety, mainly \geq C34) for
305 weakly functional \leq C50 ULC-PCs (ULCFA moiety, mainly \leq C32) (Fig. 7). This
306 substitution may be related to the continuity of acyl-CoA elongation in the FA elongation
307 cycle involving ELOVL4. The FA elongation cycle consists of four sequential reactions
308 starting from condensation by ELOVLs, then reduction by 3-ketoacyl-CoA reductase,
309 dehydration by 3-hydroxyacyl-CoA reductases, and reduction by *trans*-2-enoyl-CoA
310 reductase (4, 5). These are all ER-resident proteins and may form complexes (4, 25, 52),
311 which enables efficient and sequential progress of reactions. Since ELOVL4 is the only
312 enzyme involved in the elongation of ULC acyl-CoAs from C24 or C26 to C34–C38, it is
313 reasonable to assume that the acyl-CoA synthesized in the previous cycle enters the next
314 cycle catalyzed by the same complex, rather than dissociate from the previous complex and
315 find and associate with another complex. Thus, one C24/C26 acyl-CoA may be elongated
316 repetitively to become C34–C38 by the same ELOVL4-containing complex (Fig. 7).
317 However, it is likely that C24/C26 acyl-CoA may be elongated only up to C32 by
318 FA-elongation complexes that contain an SCA34 mutant; they would then be released from

319 the complex and used for PC synthesis. Although carriers that are heterozygous for the
320 ISQMR mutation are predicted to have half the ELOVL4 activity of normal individuals,
321 they do not develop symptoms (29–31). This may be because ULC acyl-CoAs are fully
322 elongated by the remaining WT ELOVL4 (Fig. 7). In other words, SCA34 is induced by
323 shortening of ULC PUFAs due to incomplete elongation reactions, rather than decreased
324 activity of ELOVL4.

325 In summary, this is the first biochemical analysis of SCA34 mutations, and our
326 findings suggest that the molecular mechanism underlying the pathogenesis of SCA34 is a
327 decrease in the levels and/or shortening of ULC-PCs. Furthermore, the dominant
328 inheritance mode of SCA34 is caused by the substitution of \geq C52 ULC-PCs with \leq C50
329 ULC-PCs. Another SCA subtype, namely SCA38, is caused by mutations in *ELOVL5* (53–
330 55), which is responsible for the elongation of polyunsaturated acyl-CoAs from C18 to C22
331 (Fig. 4B) (4, 5, 7). This suggests a link between SCA34 and SCA38 and raises the
332 possibility that the neural symptoms in these disorders are caused by the same or a similar
333 molecular mechanism (that is to say, the shortening of ULC-PCs). Future research is
334 needed to investigate whether SCA38 and other SCA subtypes are also accompanied by
335 changes in the quantity or quality of ULC-PCs.

336 MATERIALS AND METHODS

337 **Amino acid mapping.** Five amino acid residues of ELOVL4 that are substituted in SCA34
338 were mapped onto the crystal structure of human ELOVL7 (PDB ID: 6Y7F) using PyMOL
339 software (version 2.5.2; Schrödinger, New York, NY, USA).

340

341 **Plasmids.** The mammalian expression vectors pEFh-3×FLAG-1 (56) and pCE-puro
342 3×FLAG-1 (57) were used for the expression of N-terminally 3×FLAG-tagged proteins,
343 while the mammalian expression vector pCE-puro HA-1 (52) was used for the expression
344 of N-terminally HA-tagged protein. The pCE-puro 3×FLAG-CERS3 and pCE-puro
345 HA-ELOVL2 plasmids have been described previously (52, 58). The
346 pEFh-3×FLAG-ELOVL4 plasmid was constructed by transferring *ELOVL4* from pCE-puro
347 3×FLAG-ELOVL4 (59) to the pEFh-3×FLAG-1 vector. The *ELOVL4* mutants were
348 generated via overlap extension PCR using pCE-puro 3×FLAG-ELOVL4 plasmid as a
349 template and primers (Table 1), followed by cloning into the pEFh-3×FLAG-1 vector to
350 produce pEFh-3×FLAG-mutated ELOVL4 plasmids.

351 The all-in-one CRISPR/Cas9 vector pYU751 consists of a WT *Cas9* nuclease, a guide
352 RNA (gRNA) cloning cassette, *EGFP*, and the gene that encodes puromycin
353 *N*-acetyltransferase. This vector was constructed from the GeneArt CRISPR Nuclease
354 Vector with the OFP plasmid (Thermo Fisher Scientific, Waltham, MA, USA) by
355 incorporating the puromycin *N*-acetyltransferase gene and substituting the *ORF* reporter

356 with *EGFP*. To generate Q180P and W246G *Elovl4* KI mouse ES cells, a pair of
357 oligonucleotides (Table 2) encoding gRNAs targeting exon 4 (for Q180P) and exon 6 (for
358 W246G) of *Elovl4* were annealed and cloned into the *BaeI* site of pYU751, generating the
359 plasmids pUKA27 and pUKA16, respectively.

360

361 **Cell culture and transfection.** HEK 293T cells (RCB2202; Riken BioResource Research
362 Center, Tsukuba, Japan) and HeLa cells (RCB0007; Riken BioResource Research Center)
363 were cultured in Dulbecco's Modified Eagle's Medium containing 4,500 mg/L glucose
364 (D6429; Merck, Darmstadt, Germany) and 1,000 mg/L glucose (D6046; Merck),
365 respectively, supplemented with 10% FBS, 100 units/mL penicillin, and 100 µg/mL
366 streptomycin. HEK 293T cells were grown on collagen-coated dishes. E14tg2a mouse ES
367 cells (AES0135; Riken BioResource Research Center) were cultured in Glasgow's MEM
368 (Thermo Fisher Scientific) that was supplemented with 10% FBS, 0.1 mM MEM
369 Non-Essential Amino Acids Solution (Thermo Fisher Scientific), 1 mM sodium pyruvate
370 (Thermo Fisher Scientific), 0.1 mM 2-mercaptoethanol (FUJIFILM Wako Pure Chemical,
371 Osaka, Japan), 1,000 units/mL mouse Leukemia Inhibitory Factor (FUJIFILM Wako Pure
372 Chemical), 100 units/mL penicillin, and 100 µg/mL streptomycin, and were grown on a
373 0.1% gelatin-coated dish. All cells were cultured at 37 °C in 5% CO₂ and used in less than
374 20 passages. Transfections were performed using Lipofectamine Transfection Reagent with
375 PLUS Reagent (Thermo Fisher Scientific) according to the manufacturer's instructions.

376

377 **Indirect immunofluorescence microscopy.** HeLa cells and differentiated ES cells were
378 subjected to indirect immunofluorescence microscopy as previously described (60). Rabbit
379 anti-FLAG polyclonal antibody (1:2,000 dilution) (61), mouse anti-calnexin monoclonal
380 PM060 antibody (RRID: AB_10597560; 1:400 dilution; Medical & Biological Laboratories,
381 Tokyo, Japan), and mouse anti-class III β -tubulin monoclonal MAB1195 antibody (RRID:
382 AB_357520; 1:500 dilution; R&D Systems, Minneapolis, USA) were used as primary
383 antibodies. Alexa Fluor 488-conjugated anti-mouse IgG antibody (RRID: AB_2534069)
384 and Alexa Fluor 594-conjugated anti-rabbit IgG antibody (RRID: AB_2534073; each 1:200
385 dilution; Thermo Fisher Scientific) were used as secondary antibodies, and DAPI (1
386 $\mu\text{g}/\text{mL}$) was added simultaneously. Cover slips were mounted with ProLong Gold Antifade
387 Reagent (Thermo Fisher Scientific) and observed using a Leica DM5000B microscope
388 (Leica Microsystems, Wetzlar, Germany).

389

390 **Immunoblotting.** Immunoblotting was performed as previously described (60), using
391 rabbit anti-FLAG polyclonal antibody (1:1,000 dilution) (61) and mouse anti- α -tubulin
392 monoclonal T9026 antibody (RRID: AB_477593; 1:1,000 dilution; Merck) as primary
393 antibodies and anti-rabbit and anti-mouse IgG, HRP-linked F(ab')₂ fragments (each 1:7,500
394 dilution; GE Healthcare Life Sciences, Little Chalfont, UK) as secondary antibodies.
395 Chemiluminescence detection was performed using chemiluminescence solution; this

396 solution consisted of 100 mM Tris-HCl (pH 8.5), 0.2 mM *p*-coumaric acid (Merck), 2.5
397 mM luminol (FUJIFILM Wako Pure Chemical), and 0.002% hydrogen peroxide.

398

399 **Generation of SCA34 KI ES cells.** For homology-directed repair, the single-stranded
400 oligodeoxynucleotides (ssODNs) mElov14Q180P_ssODN and mElov14W246G_ssODN
401 were designed. Each ssODN contained the mutant sequence and bilateral homology arms
402 for homology-directed repair in ES cells (Table 3). For each ssODN, the non-target strand,
403 which was not complementary to the gRNA, was chosen to avoid heteroduplex formation
404 with gRNA (49). In the mutant sequence, mElov14Q180P_ssODN and
405 mElov14W246G_ssODN contained *ApaI* and *SphI* restriction enzyme sites, respectively;
406 these were introduced to examine the presence of mutations at the *Elov14* locus. To obtain
407 *Elov14* Q180P KI cells and W246G KI cells, ES cells were transfected with pUKA27 and
408 mElov14Q180P_ssODN (for Q180P KI cells), pUKA16 and mElov14_W246G_ssODN (for
409 W246G KI cells), or empty pYU751 vectors (as controls). Twenty-four hours after
410 transfection, the cells were treated with 2 µg/mL puromycin and incubated for another 24 h
411 to eliminate untransfected cells. The cells that survived were subsequently diluted and
412 cultured in the absence of puromycin for 9 days. Single colonies were isolated using
413 cloning rings, then expanded and stored. Genomic DNAs were extracted from the cells, and
414 the DNA fragments containing the target sites were amplified by PCR. The amplified DNA
415 fragments were digested with restriction enzymes (*ApaI* for Q180P and *SphI* for W246G) to

416 examine the presence of the mutations. Positive clones identified by restriction enzyme
417 analysis were subjected to sequence confirmation by Sanger sequencing.

418

419 **Neuronal differentiation of ES cells.** Embryoid bodies were formed by growing ES cells
420 in embryoid body formation medium; this mixture consisted of equal volumes of Advanced
421 DMEM/F12 (Thermo Fisher Scientific) and Neurobasal Medium (Thermo Fisher
422 Scientific), supplemented with 10% KnockOut Serum Replacement (Thermo Fisher
423 Scientific), 2 mM L-glutamine (Thermo Fisher Scientific), 100 units/mL penicillin, 100
424 µg/mL streptomycin, and 0.1 mM 2-mercaptoethanol. Two days later, the embryoid bodies
425 were cultured in embryoid body formation medium that was supplemented with 5 µM
426 retinoic acid. Three days later, differentiation of the embryoid bodies into neurons was
427 induced by replacing the medium with neuronal differentiation medium. This medium
428 consisted of a mixture of equal volumes of Advanced DMEM/F12 and Neurobasal Medium,
429 supplemented with 2% B-27 Supplement (Thermo Fisher Scientific), 2 mM L-glutamine,
430 100 units/mL penicillin, and 100 µg/mL streptomycin. On the following day, the embryoid
431 bodies were digested with 0.25% Trypsin/EDTA (Merck), dispersed in Leibovitz's L-15
432 Medium (Thermo Fisher Scientific) supplemented with 0.2 mg/mL DNase I (Merck), and
433 seeded onto a poly-D-lysine/laminin-coated dish in the neuronal differentiation medium for
434 an additional 4 days.

435

436 **Lipid analyses.** For the analysis of ceramides and PCs, HEK 293T cells were transfected
437 with the following combinations of plasmids: pEFh-3×FLAG-ELOVL4 (WT or one of the
438 mutants), pCE-puro 3×FLAG-CERS3, and pCE-puro HA-ELOVL2 plasmids for analysis
439 of ceramides; pEFh-3×FLAG-ELOVL4 (WT or one of the mutants) and pCE-puro
440 HA-ELOVL2 plasmids for analysis of PCs. Forty-eight hours after transfection, cells were
441 collected and subjected to lipid extraction.

442 For the extraction of ceramides from HEK 293T cells, the cells were suspended in 100
443 μL of water and mixed successively with 375 μL of chloroform/methanol/12 M formic acid
444 solution (100:200:1, v/v), 125 μL of chloroform, and 125 μL of water. After centrifugation,
445 the organic phase was recovered and treated with 71 μL of 0.5 M NaOH for 1 h at 37 °C to
446 hydrolyze ester bonds in the glycerolipids. The reaction mixture was neutralized via the
447 addition of 35.5 μL of 1 M formic acid and mixed successively with 135 μL of methanol
448 and 210 μL of water. After centrifugation, the organic phase was recovered and dried. For
449 the extraction of PCs from HEK 293T or ES cells, the cells were suspended in 100 μL of
450 water and mixed successively with 375 μL of chloroform/methanol/12 M formic acid
451 solution (100:200:1, v/v), 0.5 pmol of seven deuterium (d_7)-labeled internal standard
452 (15:0/18:1- d_7 -PC; Avanti Polar Lipids, Alabaster, USA), 125 μL of chloroform, and 125 μL
453 of water. After centrifugation, the organic phase was recovered and dried.

454 The dried lipids were suspended in a chloroform/methanol solution (1:2, v/v), and LC–
455 MS/MS analyses of ceramides and PCs were performed using an LC-coupled triple

456 quadrupole mass spectrometer Xevo TQ-S (Waters, Milford, MA, USA). Ceramides and
457 PCs extracted from HEK 293T cells were separated by LC using an ACQUITY UPLC
458 CSH C18 column (1.7 μm particle size, 2.1 \times 100 mm; Waters), and PCs extracted from ES
459 cells were separated by LC using a YMC-Triant C18 metal-free column (1.9 μm particle
460 size, 2.1 \times 50 mm; YMC, Kyoto, Japan). Lipid separation by LC was performed at a flow
461 rate of 0.3 mL/min for 25 min using a gradient system, in which mobile phase A and
462 mobile phase B were mixed as follows: 0 min, 40% B; 0–18 min, gradient to 100% B; 18–
463 23 min, 100% B; 23 min, return to 40% B; 23–25 min, 40% B. Mobile phase A consisted
464 of an acetonitrile/water solution (3:2, v/v) that contained 5 mM ammonium formate, while
465 mobile phase B consisted of an acetonitrile/2-propanol solution (1:9, v/v) that contained 5
466 mM ammonium formate. Separated lipids were ionized by electrospray ionization and
467 analyzed in positive ion mode. Quantitative analyses were performed in the multiple
468 reaction monitoring mode of the MS/MS using selected m/z values and appropriate
469 collision energies and cone voltages (Tables 4 and 5). Data analyses were performed using
470 MassLynx software (Waters). Ceramides were quantified using the external standard curve
471 generated from C30:0 ceramide (Cayman Chemical, Ann Arbor, MI, USA) and expressed
472 as the proportion of each ceramide species to the sum of all measured ceramide species
473 listed in Table 4. PCs were quantified by calculating the ratio of the peak area of each PC
474 species to that of the internal standard (15:0/18:1- d_7 -PC).

475

476 **Real-time quantitative RT-PCR.** Total RNAs were isolated from ES cells using the
477 NucleoSpin RNA Kit (Takara Bio, Kusatsu, Japan), and cDNAs were synthesized from
478 total RNAs using the PrimeScript II 1st strand cDNA Synthesis Kit (Takara Bio). Real-time
479 quantitative RT-PCR was performed using the KOD SYBR qPCR Mix (TOYOBO, Osaka,
480 Japan), cDNAs, and specific forward and reverse primers for the respective genes (Table 6).
481 The reaction was performed on a CFX96 Touch real-time PCR detection system (Bio-Rad,
482 Hercules, CA, USA). The mRNA levels were normalized to that of *Actb*.

483

484 **Quantification and statistical analysis.** Data are presented as means + SD. Tests for
485 normality of the data and outliers were not performed. Differences between groups were
486 evaluated using Dunnett's test in JMP 13 software (SAS Institute, Cary, NC, USA), and
487 *p*-values of less than 0.05 were considered to be statistically significant.

488

489 **Ethical approval.** No ethical approval was required for this study.

490

491 **ACKNOWLEDGEMENTS**

492 This work was supported by KAKENHI grants: grant numbers JP22H04986 (to A.K.) and
493 JP22H02757 (to T.S.) from the Japan Society for the Promotion of Science (JSPS) and by a
494 Grant for Basic Science Research Projects (to T.S.) from the Sumitomo Foundation.

495

496 **REFERENCES**

- 497 1. Robinson KJ, Watchon M, Laird AS. 2020. Aberrant cerebellar circuitry in the
498 spinocerebellar ataxias. *Front Neurosci* 14:707.
499 <https://doi.org/10.3389/fnins.2020.00707>
- 500 2. Sullivan R, Yau WY, O'Connor E, Houlden H. 2019. Spinocerebellar ataxia: an
501 update. *J Neurol* 266:533–544. <https://doi.org/10.1007/s00415-018-9076-4>
- 502 3. Corral-Juan M, Casquero P, Giraldo-Restrepo N, Laurie S, Martinez-Piñeiro A,
503 Mateo-Montero RC, Ispuerto L, Vilas D, Tolosa E, Volpini V, Alvarez-Ramo R,
504 Sánchez I, Matilla-Dueñas A. 2022. New spinocerebellar ataxia subtype caused by
505 *SAMD9L* mutation triggering mitochondrial dysregulation (SCA49). *Brain Commun*
506 4:fcac030. <https://doi.org/10.1093/braincomms/fcac030>
- 507 4. Kihara A. 2016. Synthesis and degradation pathways, functions, and pathology of
508 ceramides and epidermal acylceramides. *Prog Lipid Res* 63:50–69.
509 <https://doi.org/10.1016/j.plipres.2016.04.001>
- 510 5. Sassa T, Kihara A. 2014. Metabolism of very long-chain fatty acids: genes and
511 pathophysiology. *Biomol Ther* 22:83–92.
512 <https://doi.org/10.4062/biomolther.2014.017>
- 513 6. Bernert JT, Jr., Sprecher H. 1977. An analysis of partial reactions in the overall chain
514 elongation of saturated and unsaturated fatty acids by rat liver microsomes. *J Biol*
515 *Chem* 252:6736–6744. [https://doi.org/10.1016/S0021-9258\(17\)39911-8](https://doi.org/10.1016/S0021-9258(17)39911-8)

- 516 7. Ohno Y, Suto S, Yamanaka M, Mizutani Y, Mitsutake S, Igarashi Y, Sassa T, Kihara
517 A. 2010. ELOVL1 production of C24 acyl-CoAs is linked to C24 sphingolipid
518 synthesis. Proc Natl Acad Sci U S A 107:18439–18444.
519 <https://doi.org/10.1073/pnas.1005572107>
- 520 8. Beaudin M, Sellami L, Martel C, Touzel-Deschênes L, Houle G, Martineau L,
521 Lacroix K, Lavallée A, Chrestian N, Rouleau GA, Gros-Louis F, Laforce R, Jr.,
522 Dupré N. 2020. Characterization of the phenotype with cognitive impairment and
523 protein mislocalization in SCA34. Neurol Genet 6:e403.
524 <https://doi.org/10.1212/NXG.0000000000000403>
- 525 9. Bourassa CV, Raskin S, Serafini S, Teive HA, Dion PA, Rouleau GA. 2015. A new
526 *ELOVL4* mutation in a case of spinocerebellar ataxia with erythrokeratodermia.
527 JAMA Neurol 72:942–943. <https://doi.org/10.1001/jamaneurol.2015.0888>
- 528 10. Bourque PR, Warman-Chardon J, Lelli DA, LaBerge L, Kirshen C, Bradshaw SH,
529 Hartley T, Boycott KM. 2018. Novel *ELOVL4* mutation associated with
530 erythrokeratodermia and spinocerebellar ataxia (SCA 34). Neurol Genet 4:e263.
531 <https://doi.org/10.1212/NXG.0000000000000263>
- 532 11. Cadieux-Dion M, Turcotte-Gauthier M, Noreau A, Martin C, Meloche C, Gravel M,
533 Drouin CA, Rouleau GA, Nguyen DK, Cossette P. 2014. Expanding the clinical
534 phenotype associated with *ELOVL4* mutation: study of a large French-Canadian

- 535 family with autosomal dominant spinocerebellar ataxia and erythrokeratodermia.
536 JAMA Neurol 71:470–475. <https://doi.org/10.1001/jamaneurol.2013.6337>
- 537 12. Haeri G, Hajiakhoundi F, Alavi A, Ghiasi M, Munhoz RP, Rohani M. 2021.
538 Congenital ichthyosis in a case of spinocerebellar ataxia type 34: a novel presentation
539 for a known mutation. Mov Disord Clin Pract 8:275–278.
540 <https://doi.org/10.1002/mdc3.13123>
- 541 13. Mukherjee S, Roy M, Ghosh S, Guha G, Prasad Saha S, Dalal A. 2021. Rare
542 mutation in ELOVL4 gene in SCA34 and cognitive affection: Expounding the role of
543 cerebellum. Clin Neurol Neurosurg 210:106983.
544 <https://doi.org/10.1016/j.clineuro.2021.106983>
- 545 14. Ozaki K, Ansai A, Nobuhara K, Araki T, Kubodera T, Ishii T, Higashi M, Sato N,
546 Soga K, Mizusawa H, Ishikawa K, Yokota T. 2019. Prevalence and
547 clinicoradiological features of spinocerebellar ataxia type 34 in a Japanese ataxia
548 cohort. Parkinsonism Relat Disord 65:238–242.
549 <https://doi.org/10.1016/j.parkreldis.2019.05.019>
- 550 15. Ozaki K, Doi H, Mitsui J, Sato N, Iikuni Y, Majima T, Yamane K, Irioka T, Ishiura
551 H, Doi K, Morishita S, Higashi M, Sekiguchi T, Koyama K, Ueda N, Miura Y,
552 Miyatake S, Matsumoto N, Yokota T, Tanaka F, Tsuji S, Mizusawa H, Ishikawa K.
553 2015. A novel mutation in *ELOVL4* leading to spinocerebellar ataxia (SCA) with the

- 554 hot cross bun sign but lacking erythrokeratodermia: a broadened spectrum of SCA34.
555 JAMA Neurol 72:797–805. <https://doi.org/10.1001/jamaneurol.2015.0610>
- 556 16. Wang Z, Lin Z, Wang H. 2021. Progressive symmetric erythrokeratodermia with
557 spinocerebellar ataxia due to *ELOVL4* mutation in a Chinese family. Indian J
558 Dermatol Venereol Leprol 88:132. https://doi.org/10.25259/ijdv1_488_20
- 559 17. Xiao C, Binkley EM, Rexach J, Knight-Johnson A, Khemani P, Fogel BL, Das S,
560 Stone EM, Gomez CM. 2019. A family with spinocerebellar ataxia and retinitis
561 pigmentosa attributed to an *ELOVL4* mutation. Neurol Genet 5:e357.
562 <https://doi.org/10.1212/nxg.0000000000000357>
- 563 18. Nagaraja RY, Sherry DM, Fessler JL, Stiles MA, Li F, Multani K, Oroock A, Ahmad
564 M, Brush RS, Anderson RE, Agbaga MP, Deák F. 2021. W246G mutant *ELOVL4*
565 impairs synaptic plasticity in parallel and climbing fibers and causes motor defects in
566 a rat model of SCA34. Mol Neurobiol 58:4921–4943.
567 <https://doi.org/10.1007/s12035-021-02439-1>
- 568 19. Hopiavuori BR, Anderson RE, Agbaga MP. 2019. *ELOVL4*: Very long-chain fatty
569 acids serve an eclectic role in mammalian health and function. Prog Retin Eye Res
570 69:137–158. <https://doi.org/10.1016/j.preteyeres.2018.10.004>
- 571 20. Bernstein PS, Tammur J, Singh N, Hutchinson A, Dixon M, Pappas CM, Zabriskie
572 NA, Zhang K, Petrukhin K, Leppert M, Allikmets R. 2001. Diverse macular

- 573 dystrophy phenotype caused by a novel complex mutation in the *ELOVL4* gene.
574 Invest Ophthalmol Vis Sci 42:3331–3336.
- 575 21. Maugeri A, Meire F, Hoyng CB, Vink C, Van Regemorter N, Karan G, Yang Z,
576 Cremers FP, Zhang K. 2004. A novel mutation in the *ELOVL4* gene causes autosomal
577 dominant Stargardt-like macular dystrophy. Invest Ophthalmol Vis Sci 45:4263–4267.
578 <https://doi.org/10.1167/iovs.04-0078>
- 579 22. Zhang K, Kniazeva M, Han M, Li W, Yu Z, Yang Z, Li Y, Metzker ML, Allikmets R,
580 Zack DJ, Kakuk LE, Lagali PS, Wong PW, MacDonald IM, Sieving PA, Figueroa DJ,
581 Austin CP, Gould RJ, Ayyagari R, Petrukhin K. 2001. A 5-bp deletion in *ELOVL4* is
582 associated with two related forms of autosomal dominant macular dystrophy. Nat
583 Genet 27:89–93. <https://doi.org/10.1038/83817>
- 584 23. Grayson C, Molday RS. 2005. Dominant negative mechanism underlies autosomal
585 dominant Stargardt-like macular dystrophy linked to mutations in *ELOVL4*. J Biol
586 Chem 280:32521–32530. <https://doi.org/10.1074/jbc.m503411200>
- 587 24. Karan G, Yang Z, Howes K, Zhao Y, Chen Y, Cameron DJ, Lin Y, Pearson E, Zhang
588 K. 2005. Loss of ER retention and sequestration of the wild-type *ELOVL4* by
589 Stargardt disease dominant negative mutants. Mol Vis 11:657–664.
- 590 25. Okuda A, Naganuma T, Ohno Y, Abe K, Yamagata M, Igarashi Y, Kihara A. 2010.
591 Hetero-oligomeric interactions of an *ELOVL4* mutant protein: implications in the
592 molecular mechanism of Stargardt-3 macular dystrophy. Mol Vis 16:2438–2445.

- 593 26. Vasireddy V, Vijayasathy C, Huang J, Wang XF, Jablonski MM, Petty HR, Sieving
594 PA, Ayyagari R. 2005. Stargardt-like macular dystrophy protein ELOVL4 exerts a
595 dominant negative effect by recruiting wild-type protein into aggresomes. *Mol Vis*
596 11:665–676.
- 597 27. Esteve-Rudd J, Hazim RA, Diemer T, Paniagua AE, Volland S, Umapathy A,
598 Williams DS. 2018. Defective phagosome motility and degradation in cell
599 nonautonomous RPE pathogenesis of a dominant macular degeneration. *Proc Natl*
600 *Acad Sci U S A* 115:5468–5473. <https://doi.org/10.1073/pnas.1709211115>
- 601 28. Kuny S, Cho WJ, Dimopoulos IS, Sauvé Y. 2015. Early onset ultrastructural and
602 functional defects in RPE and photoreceptors of a Stargardt-like macular dystrophy
603 (STGD3) transgenic mouse model. *Invest Ophthalmol Vis Sci* 56:7109–7121.
604 <https://doi.org/10.1167/iovs.15-17567>
- 605 29. Aldahmesh MA, Mohamed JY, Alkuraya HS, Verma IC, Puri RD, Alaiya AA, Rizzo
606 WB, Alkuraya FS. 2011. Recessive mutations in *ELOVL4* cause ichthyosis,
607 intellectual disability, and spastic quadriplegia. *Am J Hum Genet* 89:745–750.
608 <https://doi.org/10.1016/j.ajhg.2011.10.011>
- 609 30. Diociaiuti A, Martinelli D, Nicita F, Cesario C, Pisaneschi E, Macchiaiolo M, Rossi S,
610 Condorelli AG, Zambruno G, El Hachem M. 2021. Two Italian patients with
611 *ELOVL4*-related neuro-ichthyosis: expanding the genotypic and phenotypic spectrum

612 and ultrastructural characterization. Genes 12:343.
613 <https://doi.org/10.3390/genes12030343>

614 31. Mir H, Raza SI, Touseef M, Memon MM, Khan MN, Jaffar S, Ahmad W. 2014. A
615 novel recessive mutation in the gene ELOVL4 causes a neuro-ichthyotic disorder
616 with variable expressivity. BMC Med Genet 15:25.
617 <https://doi.org/10.1186/1471-2350-15-25>

618 32. Sherry DM, Hopiavuori BR, Stiles MA, Rahman NS, Ozan KG, Deak F, Agbaga MP,
619 Anderson RE. 2017. Distribution of ELOVL4 in the developing and adult mouse
620 brain. Front Neuroanat 11:38. <https://doi.org/10.3389/fnana.2017.00038>

621 33. Bennett LD, Brush RS, Chan M, Lydic TA, Reese K, Reid GE, Busik JV, Elliott MH,
622 Anderson RE. 2014. Effect of reduced retinal VLC-PUFA on rod and cone
623 photoreceptors. Invest Ophthalmol Vis Sci 55:3150–3157.
624 <https://doi.org/10.1167/iovs.14-13995>

625 34. Harkewicz R, Du H, Tong Z, Alkuraya H, Bedell M, Sun W, Wang X, Hsu YH,
626 Esteve-Rudd J, Hughes G, Su Z, Zhang M, Lopes VS, Molday RS, Williams DS,
627 Dennis EA, Zhang K. 2012. Essential role of ELOVL4 protein in very long chain
628 fatty acid synthesis and retinal function. J Biol Chem 287:11469–11480.
629 <https://doi.org/10.1074/jbc.m111.256073>

630 35. Li W, Sandhoff R, Kono M, Zerfas P, Hoffmann V, Ding BC, Proia RL, Deng CX.
631 2007. Depletion of ceramides with very long chain fatty acids causes defective skin

632 permeability barrier function, and neonatal lethality in ELOVL4 deficient mice. *Int J*
633 *Biol Sci* 3:120–128. <https://doi.org/10.7150/ijbs.3.120>

634 36. Vasireddy V, Uchida Y, Salem N, Jr., Kim SY, Mandal MN, Reddy GB, Bodepudi R,
635 Alderson NL, Brown JC, Hama H, Dlugosz A, Elias PM, Holleran WM, Ayyagari R.
636 2007. Loss of functional ELOVL4 depletes very long-chain fatty acids ($\geq C28$) and
637 the unique ω -O-acylceramides in skin leading to neonatal death. *Hum Mol Genet*
638 16:471–482. <https://doi.org/10.1093/hmg/ddl480>

639 37. Rabionet M, Bayerle A, Jennemann R, Heid H, Fuchser J, Marsching C, Porubsky S,
640 Bolenz C, Guillou F, Gröne HJ, Gorgas K, Sandhoff R. 2015. Male meiotic
641 cytokinesis requires ceramide synthase 3-dependent sphingolipids with unique
642 membrane anchors. *Hum Mol Genet* 24:4792–4808.
643 <https://doi.org/10.1093/hmg/ddv204>

644 38. McMahon A, Lu H, Butovich IA. 2014. A role for ELOVL4 in the mouse meibomian
645 gland and sebocyte cell biology. *Invest Ophthalmol Vis Sci* 55:2832–2840.
646 <https://doi.org/10.1167/iovs.13-13335>

647 39. Miyamoto M, Sassa T, Sawai M, Kihara A. 2020. Lipid polarity gradient formed by
648 ω -hydroxy lipids in tear film prevents dry eye disease. *eLife* 9:e53582.
649 <https://doi.org/10.7554/elife.53582>

- 650 40. Otsuka K, Sawai-Ogawa M, Kihara A. 2022. Formation of fatty alcohols-components
651 of meibum lipids-by the fatty acyl-CoA reductase FAR2 is essential for dry eye
652 prevention. *FASEB J* 36:e22216. <https://doi.org/10.1096/fj.202101733r>
- 653 41. Sassa T, Tadaki M, Kiyonari H, Kihara A. 2018. Very long-chain tear film lipids
654 produced by fatty acid elongase ELOVL1 prevent dry eye disease in mice. *FASEB J*
655 32:2966–2978. <https://doi.org/10.1096/fj.201700947r>
- 656 42. Sawai M, Watanabe K, Tanaka K, Kinoshita W, Otsuka K, Miyamoto M, Sassa T,
657 Kihara A. 2021. Diverse meibum lipids produced by Awat1 and Awat2 are important
658 for stabilizing tear film and protecting the ocular surface. *iScience* 24:102478.
659 <https://doi.org/10.1016/j.isci.2021.102478>
- 660 43. Poulos A, Sharp P, Johnson D, Easton C. 1988. The occurrence of polyenoic very
661 long chain fatty acids with greater than 32 carbon atoms in molecular species of
662 phosphatidylcholine in normal and peroxisome-deficient (Zellweger's syndrome)
663 brain. *Biochem J* 253:645–650. <https://doi.org/10.1042/bj2530645>
- 664 44. Robinson BS, Johnson DW, Poulos A. 1990. Unique molecular species of
665 phosphatidylcholine containing very-long-chain (C24–C38) polyenoic fatty acids in
666 rat brain. *Biochem J* 265:763–767. <https://doi.org/10.1042/bj2650763>
- 667 45. Nie L, Pascoa TC, Pike ACW, Bushell SR, Quigley A, Ruda GF, Chu A, Cole V,
668 Speedman D, Moreira T, Shrestha L, Mukhopadhyay SMM, Burgess-Brown NA,
669 Love JD, Brennan PE, Carpenter EP. 2021. The structural basis of fatty acid

- 670 elongation by the ELOVL elongases. *Nat Struct Mol Biol* 28:512–520.
671 <https://doi.org/10.1038/s41594-021-00605-6>
- 672 46. Mizutani Y, Sun H, Ohno Y, Sassa T, Wakashima T, Obara M, Yuyama K, Kihara A,
673 Igarashi Y. 2013. Cooperative synthesis of ultra long-chain fatty acid and ceramide
674 during keratinocyte differentiation. *PLoS One* 8:e67317.
675 <https://doi.org/10.1371/journal.pone.0067317>
- 676 47. Yamamoto M, Sassa T, Kyono Y, Uemura H, Kugo M, Hayashi H, Imai Y,
677 Yamanishi K, Kihara A. 2021. Comprehensive stratum corneum ceramide profiling
678 reveals reduced acylceramides in ichthyosis patient with *CERS3* mutations. *J*
679 *Dermatol* 48:447–456. <https://doi.org/10.1111/1346-8138.15725>
- 680 48. Kim M, Habiba A, Doherty JM, Mills JC, Mercer RW, Huettner JE. 2009. Regulation
681 of mouse embryonic stem cell neural differentiation by retinoic acid. *Dev Biol*
682 328:456–471. <https://doi.org/10.1016/j.ydbio.2009.02.001>
- 683 49. Richardson CD, Ray GJ, DeWitt MA, Curie GL, Corn JE. 2016. Enhancing
684 homology-directed genome editing by catalytically active and inactive CRISPR-Cas9
685 using asymmetric donor DNA. *Nat Biotechnol* 34:339–344.
686 <https://doi.org/10.1038/nbt.3481>
- 687 50. Deák F, Anderson RE, Fessler JL, Sherry DM. 2019. Novel cellular functions of very
688 long chain-fatty acids: insight from ELOVL4 mutations. *Front Cell Neurosci* 13:428.
689 <https://doi.org/10.3389/fncel.2019.00428>

- 690 51. Yeboah GK, Lobanova ES, Brush RS, Agbaga MP. 2021. Very long chain fatty
691 acid-containing lipids: a decade of novel insights from the study of ELOVL4. *J Lipid*
692 *Res* 62:100030. <https://doi.org/10.1016/j.jlr.2021.100030>
- 693 52. Ikeda M, Kanao Y, Yamanaka M, Sakuraba H, Mizutani Y, Igarashi Y, Kihara A.
694 2008. Characterization of four mammalian 3-hydroxyacyl-CoA dehydratases
695 involved in very long-chain fatty acid synthesis. *FEBS Lett* 582:2435–2440.
696 <https://doi.org/10.1016/j.febslet.2008.06.007>
- 697 53. Borroni B, Di Gregorio E, Orsi L, Vaula G, Costanzi C, Tempia F, Mitro N, Caruso
698 D, Manes M, Pinessi L, Padovani A, Brusco A, Boccone L. 2016. Clinical and
699 neuroradiological features of spinocerebellar ataxia 38 (SCA38). *Parkinsonism Relat*
700 *Disord* 28:80–86. <https://doi.org/10.1016/j.parkreldis.2016.04.030>
- 701 54. Di Gregorio E, Borroni B, Giorgio E, Lacerenza D, Ferrero M, Lo Buono N, Ragusa
702 N, Mancini C, Gausson M, Calcia A, Mitro N, Hoxha E, Mura I, Coviello DA, Moon
703 YA, Tesson C, Vaula G, Couarch P, Orsi L, Duregon E, Papotti MG, Deleuze JF,
704 Imbert J, Costanzi C, Padovani A, Giunti P, Maillet-Vioud M, Durr A, Brice A,
705 Tempia F, Funaro A, Boccone L, Caruso D, Stevanin G, Brusco A. 2014. *ELOVL5*
706 mutations cause spinocerebellar ataxia 38. *Am J Hum Genet* 95:209–217.
707 <https://doi.org/10.1016/j.ajhg.2014.07.001>
- 708 55. Gazulla J, Orduna-Hospital E, Benavente I, Rodríguez-Valle A, Osorio-Caicedo P,
709 Alvarez-de Andrés S, García-González E, Fraile-Rodrigo J, Fernández-Tirado FJ,

- 710 Berciano J. 2020. Contributions to the study of spinocerebellar ataxia type 38
711 (SCA38). *J Neurol* 267:2288–2295. <https://doi.org/10.1007/s00415-020-09840-1>
- 712 56. Jojima K, Edagawa M, Sawai M, Ohno Y, Kihara A. 2020. Biosynthesis of the
713 anti-lipid-microdomain sphingoid base 4,14-sphingadiene by the ceramide desaturase
714 FADS3. *FASEB J* 34:3318–3335. <https://doi.org/10.1096/fj.201902645r>
- 715 57. Kihara A, Anada Y, Igarashi Y. 2006. Mouse sphingosine kinase isoforms SPHK1a
716 and SPHK1b differ in enzymatic traits including stability, localization, modification,
717 and oligomerization. *J Biol Chem* 281:4532–4539.
718 <https://doi.org/10.1074/jbc.m510308200>
- 719 58. Ohno Y, Nakamichi S, Ohkuni A, Kamiyama N, Naoe A, Tsujimura H, Yokose U,
720 Sugiura K, Ishikawa J, Akiyama M, Kihara A. 2015. Essential role of the cytochrome
721 P450 CYP4F22 in the production of acylceramide, the key lipid for skin permeability
722 barrier formation. *Proc Natl Acad Sci U S A* 112:7707–7712.
723 <https://doi.org/10.1073/pnas.1503491112>
- 724 59. Ohno Y, Kamiyama N, Nakamichi S, Kihara A. 2017. PNPLA1 is a transacylase
725 essential for the generation of the skin barrier lipid ω -O-acylceramide. *Nat Commun*
726 8:14610. <https://doi.org/10.1038/ncomms14610>
- 727 60. Kitamura T, Takagi S, Naganuma T, Kihara A. 2015. Mouse aldehyde dehydrogenase
728 ALDH3B2 is localized to lipid droplets via two C-terminal tryptophan residues and
729 lipid modification. *Biochem J* 465:79–87. <https://doi.org/10.1042/bj20140624>

730 61. Kitamura T, Seki N, Kihara A. 2017. Phytosphingosine degradation pathway includes
731 fatty acid α -oxidation reactions in the endoplasmic reticulum. Proc Natl Acad Sci U S
732 A 114:E2616–E2623. <https://doi.org/10.1073/pnas.1700138114>
733

734

735 **FIG 1** Multiple alignment of ELOVL1–7. Amino acid sequences of human ELOVL1–
736 7 proteins were aligned using Clustal Omega (<https://www.ebi.ac.uk/Tools/msa/clustalo/>).
737 The numbers in the right-hand margin refer to the adjacent amino acid residues. Amino
738 acid residues conserved in all seven isozymes are indicated by black boxes, while residues
739 conserved in five or six isozymes are indicated by gray boxes. SCA34-substituted residues
740 in ELOVL4 and corresponding residues in ELOVL7 are indicated by cyan and orange
741 boxes, respectively. The catalytically important histidine box is marked by a red rectangle.

742

743 **FIG 2** Positions of the amino acid residues of ELOVL4 that are substituted in SCA34
744 mapped to the crystal structure of ELOVL7. Five amino acid residues of ELOVL4 that are
745 substituted in SCA34 (magenta) mapped on the ribbon diagram of the human ELOVL7
746 structure with the bound acyl-CoA analog containing the C20:0 FA moiety (PDB: 6Y7F)
747 (45). The catalytically important histidine box (H-box) is shown in lime green.

748

749 **FIG 3** Localization of ELOVL4 SCA34 mutant proteins in the ER. HeLa cells were
750 transfected with a vector or each of the 3×*FLAG-ELOVL4*-encoding plasmids: WT and five
751 SCA34 mutants (L168F, I171T, Q180P, T233M, and W246G). Twenty-four hours after
752 transfection, the cells were fixed and subjected to indirect immunofluorescence microscopy

753 using anti-FLAG antibody (red) and anti-calnexin antibody (green), which mark the ER.
754 Nuclei were stained with DAPI (blue). Scale bar, 10 μ m.

755

756 **FIG 4** Incomplete elongation of ULC PUFAs by ELOVL4 SCA34 mutants. (A)
757 Structures of a representative ULC PUFA-containing ceramide (upper) and ULC-PC
758 (lower): a ceramide that contains C32:6 FA (upper) and a PC that contains FAs (lower)
759 making a total of C50:7 (C32:6 FA in the *sn*-1 position plus C18:1 in the *sn*-2 position). (B)
760 Schematic representations of PUFA elongation pathways (*n*-6 and *n*-3 series). Linoleic
761 acid (C18:2 n -6) and α -linolenic acid (C18:3 n -3) are subject to a series of reactions,
762 including desaturation, elongation by ELOVL isozymes, and β -oxidation, and some of the
763 products are elongated to ULC PUFAs by ELOVL4. The letter E denotes ELOVL
764 isozymes and font size reflects the relative strength of their activities. (C–G) HEK 293T
765 cells were transfected with a vector or each of the 3 \times FLAG-ELOVL4-encoding plasmids
766 (WT, L168F, I171T, Q180P, T233M, W246G, and R216X), together with
767 3 \times FLAG-CERS3- and HA-ELOVL2-encoding plasmids (C–E) or HA-ELOVL2-encoding
768 plasmid (F and G) for 48 h. (C and F) Total lysates prepared from the transfected cells were
769 separated by SDS-PAGE, followed by immunoblotting with anti-FLAG, anti-HA, and
770 anti- α -tubulin (for loading control) antibodies. (D, E, G) Lipids were extracted from the
771 transfected cells, and ceramides (D and E) or PCs (G) containing the indicated FA moiety
772 were analyzed by LC–MS/MS. PC species are expressed as the sum of the chain-length and

773 the number of double bonds of two constituent FAs. (D and G) Heatmaps presenting the
774 levels of ceramide (D) or PC (G) species in each kind of ELOVL4 mutant-expressing cell
775 relative to those in ELOVL4 WT-expressing cells ($n = 3$ independent cell cultures). (E)
776 Percentages of the C32:6 and C38:6 ceramides among the total ceramides quantified in (D).
777 Values represent means + SD ($n = 3$ independent cell cultures). Significant differences in
778 comparison to ELOVL4 WT-expressing cells ($*P < 0.05$; $**P < 0.01$; Dunnett's test) are
779 indicated.

780

781 **FIG 5** Differentiation of ES cells into neurons induces *Elovl4* expression and ULC-PC
782 production. ES cells were differentiated into neurons in neuronal differentiation medium for
783 5 days. The cells were harvested for RNA and lipid extractions prior to the initiation of
784 differentiation (day 0), on day 1, and on day 5. (A) On days 0, 1, and 5, bright-field images
785 of live cells were captured, then the cells were fixed and subjected to indirect
786 immunofluorescence microscopy using anti-class III β -tubulin antibody (green). Nuclei
787 were stained with DAPI (blue). Scale bars, 100 μm (day 0) and 25 μm (days 1 and 5). (B)
788 Total RNAs were prepared from the cells on days 0, 1, and 5, and were subjected to
789 real-time quantitative RT-PCR using specific primers for *Elovl4* or *Actb*. Values presented
790 are the mean (+ SD) levels of *Elovl4* mRNA relative to those of *Actb* (3 independent cell
791 cultures). (C) Lipids were extracted from the cells on days 0, 1, and 5, and ULC-PCs were

792 analyzed by LC–MS/MS. Values presented are mean (+ SD) levels of ULC-PCs (3
793 independent cell cultures).

794

795

796 **FIG 6** Incomplete elongation of ULC PUFAs in *ELOVL4* Q180P and W246G KI
797 neurons. (A) The gene structure of *Elovl4* and sequence chromatograms of the Q180P and
798 W246G mutations in control, heterozygous Q180P, heterozygous W246G, and
799 homozygous W246G KI ES cells. (B and C) Control and KI ES cells were differentiated
800 into neurons for 1 (B) and 5 days (B and C). (B) Lipids were extracted and the PC species
801 C44:5–C56:7, which are expressed according to the sum of their chain length and the
802 number of double bonds in their two constituent FAs, were analyzed by LC–MS/MS.
803 Values in the left panels on days 1 and 5 represent mean (+ SD) levels of PCs (3
804 independent cell cultures), with each PC species being color-coded. Values in the right
805 panels on days 1 and 5 represent the percentages of \geq C52 ULC-PCs among the sum of
806 C44:5–C56:7 PCs (3 independent cell cultures). Significant differences from control cells
807 ($*P < 0.05$; $**P < 0.01$; Dunnett's test) are indicated. (C) Total RNAs were prepared from
808 the cells and subjected to real-time quantitative RT-PCR using specific primers for *Elovl2*,
809 *Elovl4*, *Elovl5*, *Tubb3*, or *Actb*. Values presented are mean (+ SD) levels of each mRNA
810 relative to those of *Actb* and expressed as a ratio to the control cells (3 independent cell
811 cultures). Significant differences from control cells ($*P < 0.05$; $**P < 0.01$; Dunnett's test)
812 are indicated. Het, heterozygous; Homo, homozygous.

813

814 **FIG 7** Model for the dominant mode of inheritance in SCA34. One C24/C26
815 acyl-CoA synthesized by ELOVL5 and ELOVL2 is elongated by the same WT or SCA34
816 mutant ELOVL4 protein (black arrows). In normal cases, in which both *ELOVL4* alleles are
817 WT, C24/C26 acyl-CoAs are elongated to become C34–C38; this process produces highly
818 functional ULC-PCs. In patients with ISQMR, in whom both *ELOVL4* alleles are ISQMR
819 mutants, C24/C26 acyl-CoAs cannot be elongated by the ISQMR mutant protein (gray
820 arrows with crosses), and there is no production of \geq C28 ULC-PCs. In ISQMR carriers, in
821 whom one allele is WT and the other allele is an ISQMR mutant, all C24/C26 acyl-CoAs
822 are elongated by the remaining WT protein; thus, normal levels of highly functional
823 ULC-PCs may be produced. In patients with SCA34 in whom one allele is WT and the
824 other allele is an SCA34 mutant, a proportion of C24/C26 acyl-CoAs are elongated
825 normally to C34–C38 by the WT protein. The remaining proportion is elongated by the
826 SCA34 protein only up to C32, thereby producing weakly functional ULC-PCs. Gray
827 arrows indicate reduced elongation.

828

829 **TABLE 1** Oligonucleotides used for the generation of mutated *ELOVL4* plasmids.

Primer name	Sequence
ELOVL4_F	5'- <u>GGATCC</u> ATGGGGCTCCTGGACTCGGAGCCGG-3' (<i>Bam</i> HI)
ELOVL4_R	5'-TTAATCTCCTTTTGCTTTTCCATTTTTC-3'
E4_L168F-1	5'-TGTTTACCTTCTGGTGGATTGGAATTAAGTG-3'
E4_L168F-2	5'-CAATCCACCAGAAGGTAAACATCGTACAGTG-3'
E4_I171T-1	5'-TTGTGGTGGACTGGAATTAAGTGGGTTGCAG-3'
E4_I171T-2	5'-CTTAATTCCAGTCCACCACAAGGTAAACATC-3'
E4_Q180P-1	5'-GCAGGAGGACCAGCATTTTTTTGGAGCCCAGTTG-3'
E4_Q180P-2	5'-AAAAAATGCTGGTCCTCCTGCAACCCACTTAATTC-3'
E4_T233M-1	5'-ATTGGGCACATGGCACTGTCTCTTTACACTG-3'
E4_T233M-2	5'-AGACAGTGCCATGTGCCCAATGGTCACATGG-3'
E4_W246G-1	5'-CTTCCCCAAAGGGATGCACTGGGCTCTAATTG-3'
E4_W246G-2	5'-CAGTGCATCCCTTTGGGGAAGGGGCAGTCAG-3'
E4_R216X-1	5'-TTGGTGGAAATGATACCTGACTATGTTGCAAC-3'
E4_R216X-2	5'-GTCAGGTATCATTTCCACCAAAGATATTTCTG-3'

830 The restriction enzyme *Bam*HI used for cloning into the expression vector is noted in

831 parentheses, with its sequence underlined.

832 **TABLE 2** Oligonucleotides used for the generation of CRISPR/Cas9 plasmids.

Oligonucleotide name	Sequence	Plasmid name
mElov14_Q180P-gRNA_ F1	5'-GAAAGGTGGGTCCCTCACCTGTTTT-3'	pUKA27
mElov14_Q180P-gRNA_ R1	5'-AGGTGAGGGACCCACCTTTCCGGTG-3'	
mElov14_W246G-gRNA_ _F1	5'-AGAGCCCAGTGCATCCACTTGTTTT-3'	pUKA16
mElov14_W246G-gRNA_ _R1	5'-AAGTGGATGCACTGGGCTCTCGGTG-3'	

833

834 **TABLE 3** ssODNs used for homology-directed repair

<i>Elovl4</i> mutation	Sequence
Q180P	5'-CTAGGTAAACCTACTCCCACCCACATGGGGGTTTCAGAC AGAAAGGTGGGTCCCTCACCGGGCCCTCCAGCCACCCAC TTGATTCCAATCCACCACAGAGTGAACATGGTGCAGTGGT GGT-3' (<i>ApaI</i>)
W246G	5'-GTAGAAGTTGAGGAAGAGGAAGATGAAGCTGATGGCG TAGGCGATCAGAGCCCAGTGCATGCCCTTGGGGAAGGGG CAGTCGGTGTAGAGAGACAGTGCTGTGTGTCCGATGGTC ACGTGGAA-3' (<i>SphI</i>)

835 The restriction enzymes used for genotyping KI cells are noted in parentheses, with their

836 sequences underlined.

837

838 **TABLE 4** Selected m/z values and collision energies for the detection of ceramide species

839 in the LC–MS/MS analysis.

Acyl chain	Precursor ions (Q1, m/z)		Product ion (Q3, m/z)	Collision energy (eV)
	$[M - H_2O + H]^+$	$[M + H]^+$		
C18:0	548.6	566.6	264.3	20
C20:0	576.6	594.6	264.3	20
C22:0	604.6	622.6	264.3	25
C24:0	632.6	650.6	264.3	30
C26:0	660.7	678.7	264.3	30
C28:0	688.7	706.7	264.3	30
C30:0	716.7	734.7	264.3	35
C32:0	744.8	762.8	264.3	40
C34:0	772.8	790.8	264.3	40
C18:1	546.6	564.6	264.3	20
C20:1	574.6	592.6	264.3	20
C22:1	602.6	620.6	264.3	25
C24:1	630.6	648.6	264.3	30
C26:1	658.7	676.7	264.3	30
C28:1	686.7	704.7	264.3	30
C30:1	714.7	732.7	264.3	35
C32:1	742.8	760.8	264.3	35
C34:1	770.8	788.8	264.3	40
C36:1	798.8	816.8	264.3	40
C38:1	826.8	844.8	264.3	40
C24:4	624.6	642.6	264.3	30
C26:4	652.7	670.7	264.3	30

C28:4	680.7	698.7	264.3	30
C30:4	708.7	726.7	264.3	35
C32:4	736.8	754.8	264.3	35
C34:4	764.8	782.8	264.3	40
C36:4	792.8	810.8	264.3	40
C38:4	820.9	838.9	264.3	40
C30:5	706.7	724.7	264.3	35
C32:5	734.7	752.7	264.3	35
C34:5	762.8	780.8	264.3	40
C36:5	790.8	808.8	264.3	40
C38:5	818.8	836.8	264.3	40
C30:6	704.7	722.7	264.3	35
C32:6	732.7	750.7	264.3	35
C34:6	760.8	778.8	264.3	40
C36:6	788.8	806.8	264.3	40
C38:6	816.8	834.8	264.3	40

840

841 **TABLE 5** Selected m/z values for the detection of PC species in the LC–MS/MS analysis.

Sum of two acyl chains	Precursor ion (Q1, m/z)	Product ion (Q3, m/z)
C33:1- d_7	753.5	184.0
C44:5	892.8	184.0
C44:6	890.8	184.0
C44:7	888.7	184.0
C46:5	920.8	184.0
C46:6	918.8	184.0
C46:7	916.8	184.0
C48:5	948.8	184.0
C48:6	946.8	184.0
C48:7	944.8	184.0
C50:5	976.9	184.0
C50:6	974.9	184.0
C50:7	972.8	184.0
C52:5	1004.9	184.0
C52:6	1002.9	184.0
C52:7	1000.9	184.0
C54:5	1032.9	184.0
C54:6	1030.9	184.0
C54:7	1028.9	184.0
C56:5	1061.0	184.0
C56:6	1059.0	184.0
C56:7	1056.9	184.0

842 Collision energy and cone voltage were 30 eV and 15 V, respectively.

843

844 **TABLE 6** Primers used for real-time quantitative RT-PCR.

Primer name	Sequence
mElovl4-rt_F1	5'-ACGTGATCATGTACTCCTACTATGG-3'
mElovl4-rt_R1	5'-CCGTTTCGATGAGATAACCATTCGTGG-3'
mTubb3-rt_F3	5'-GAGGCCTCCTCTCACAAGTATGTGC-3'
mTubb3-rt_R3	5'-GTTGCCAGCACCCTCTGACCAAAG-3'
mElovl2-rt_F	5'-GCTGGTCATCCTGTTCTTAAACTTC-3'
mElovl2-rt_R	5'-TTATTGAGCCTTCTTGTCCGTCATG-3'
mElovl5-rt_F2	5'-TCGGGTGGCTGTTCTTCCAGATTGG-3'
mElovl5-rt_R	5'-AGGGAAGCTGTTGGTGTGTCCGTTG-3'
Mouse_Actb_primer	Mouse Housekeeping Gene Primer Set (Takara Bio)

845

Fig. 1

ELOVL1 MEAVVNLYQEVMKHADPRIQGYPLMGSPLL-MTSILLTYVYF 41
ELOVL2 MEHLKAFDDEINAFLDNMFGRDSRVRGWFM LDSYLP-TFFLTVMYLLS 48
ELOVL3 MVTAMNVSHEVNQLFQPYNFEL---SK--DMRPFEEYWATSFPIALIYLVL 47
ELOVL4 MGLLDSEPGSVLNVVSTALNDTVEFYRWTWSIADKRVENWPLMQSPWP-TLSISTLYLLF 59
ELOVL5 MEHFDASLSTYFKALLGPRDTRVKGWFLLDNYIP-TFICSVIYLLI 45
ELOVL6 MNMSV---LTLQEYEFKQFNEN--EAIQWMQENWKKSF LFSALYAAF 43
ELOVL7 MAFSDLTSRTVHLYDNWIKDADPRVEDWLLMSSPLP-QTILLGFYVYF 47

ELOVL1 VLSLGPRI MANRKP FQLRGFMIVYNFSLVALS L Y-----IVYEFLMSGWLSTYTWR C 93
ELOVL2 I-WLGNKYMKNRPALSLRGILTLYNLGITLLSAY-----MLAELILSTWEGGYNLO C 99
ELOVL3 I-AVGQNYMKERKGFNLQGPLILWSFCLAIFSILGAVRMWGI MGTVLLTGGLKQ---TVC 103
ELOVL4 V-WLGPKWMKDREPFQMRVLVLIYNF GMVLLNLF-----IFRELFMGSYNAGYSYIC 110
ELOVL5 V-WLGPKYMRNKQPFSCRGILVYVNLGLTLLS L Y-----MFCELVTGVWEGKYNFFC 96
ELOVL6 I-FGGRHLMNKRAK FELRKPLVLSLTLAVFSIFGALRTGAYMVYILMTKGLKQ---SVC 99
ELOVL7 VTSLGPKLMENRKP FELKKAMITYNFFIVLFSVY-----MCYEFVMSGWGIGYSFRC 99

ELOVL1 DPVDYSNSPEALRMVRVAWLFLFSKFI E LMDTVIFILRKKDGQVTF LHV FHH SVLPWSWW 153
ELOVL2 QDLTS-AGEADIRVAKVLWYYF S KSV EFLDTIFFVLRKKTSQITFLHVYHHASMFNIWW 158
ELOVL3 FINFIDNST---VKFWSWVLLSKVIE LGDTAFIILRKR--PLIFIHWHYHHSTVLVYTS 157
ELOVL4 QSDVYSNNVHEVRIAAALWYFVSKGVEYLDTVFFILRKKNNQVSFLHVYHHCTMFTLWW 170
ELOVL5 QGTRT-AGESDMKIIRVLWYYF SKLIEFMDTFFFILRKNNHQITVLHVYHHASMLNIWW 155
ELOVL6 DQGFYNGPV---SKFWAYAFVLSKAP E LGDTIFFIILRKKQ--KLIFLHWYHHITVLLYSW 153
ELOVL7 DIVDYSRSPALRMARTCWLYYFSKFI E LLDTIFFVLRKKNSQVTF LHV FHH T IMPWTWW 159

ELOVL1 WGVK IAPGGMG SFHAMINSSVHVIMYLYYGLS AFGPVAQPYLWKKHMTAIQLIQFVLVS 213
ELOVL2 CVLNWIPCQGSFFGPTLNSFIHILMYSY YGLSVF-PSMHKYLWKKYL TQAQLVQFVLT I 217
ELOVL3 FGYKNKVPAGGW F-VTMNFGVHAIMYTY YTLKAANVKPK--MLPMLITSLQILQMFVGA 214
ELOVL4 IGIKWVAGGQAF FGAQLNSFIHVIMYSY YGLTAFGPWIQKYLWKKRYL TMLQLIQFHVTI 230
ELOVL5 FVMNWVPCGHSYFGATLNSFIHVL MYSY YGLSSV-PSMRPYLWKKYITQGLLOFVLT I 214
ELOVL6 YSYKDMVAGGGWF-MTMNYGVHAVMYSY YALRAAGFRVSR--KFAMFITLSQITQMLMGC 210
ELOVL7 FGVKFAAGGLGTFHALLNTAVHVMYSY YGLSALGPAYQKYLWKKYL TSLQLVQFVIVA 219

ELOVL1 LHS---QYYFMSSCNYQYPV I IH-LIWMYGTIFFM LFSNFWYHSYTKGKRLPRAL--- 265
ELOVL2 THM---S-AVVKPCGF--PFGCLIFQSSYMLTLVILFLN FYVQTYRKKPKMKKDMQEP P- 270
ELOVL3 IVSILTYIWRQDQGCHTTMEH-LFWSF ILY-MTYFIFLFAHFFCQTYIRPKVKAKTKSQ 270
ELOVL4 GHTA---L-SLYTD CPF--PKMHWALIA Y AISFIFLFLN FYIRTYKEPKKPKAGKTA-- 282
ELOVL5 IQTS---C-GVIWPC TF--PLGWLYFQIGY MISLIALFTNFYIQTYNKKGASRRKDHLKD 268
ELOVL6 VVNYLVFCWMQHDQCHSHFQ N-IFWSSLMY-LSYLVLFCHFFFEAYIGKMRKTTKAE 265
ELOVL7 IHS---QFFFMEDCKYQFPV F AC-IIMSY S FMFL LFLHF WYRAYTKGQRLPKTV--- 271

ELOVL1 -QQN-GAPGIAKVKAN 279
ELOVL2 --AG-KEVKNGF SKAYFTAANGVMNKK--AQ 296
ELOVL3 270
ELOVL4 -MNGISANGVSKSEKQLMIENGKKQKNGKAKGD 314
ELOVL5 HQNGSMAAVNGHTNSFSPLENNVKPRK--LRKD 299
ELOVL6 265
ELOVL7 -KNG-TCKNKDN 281

Fig. 2

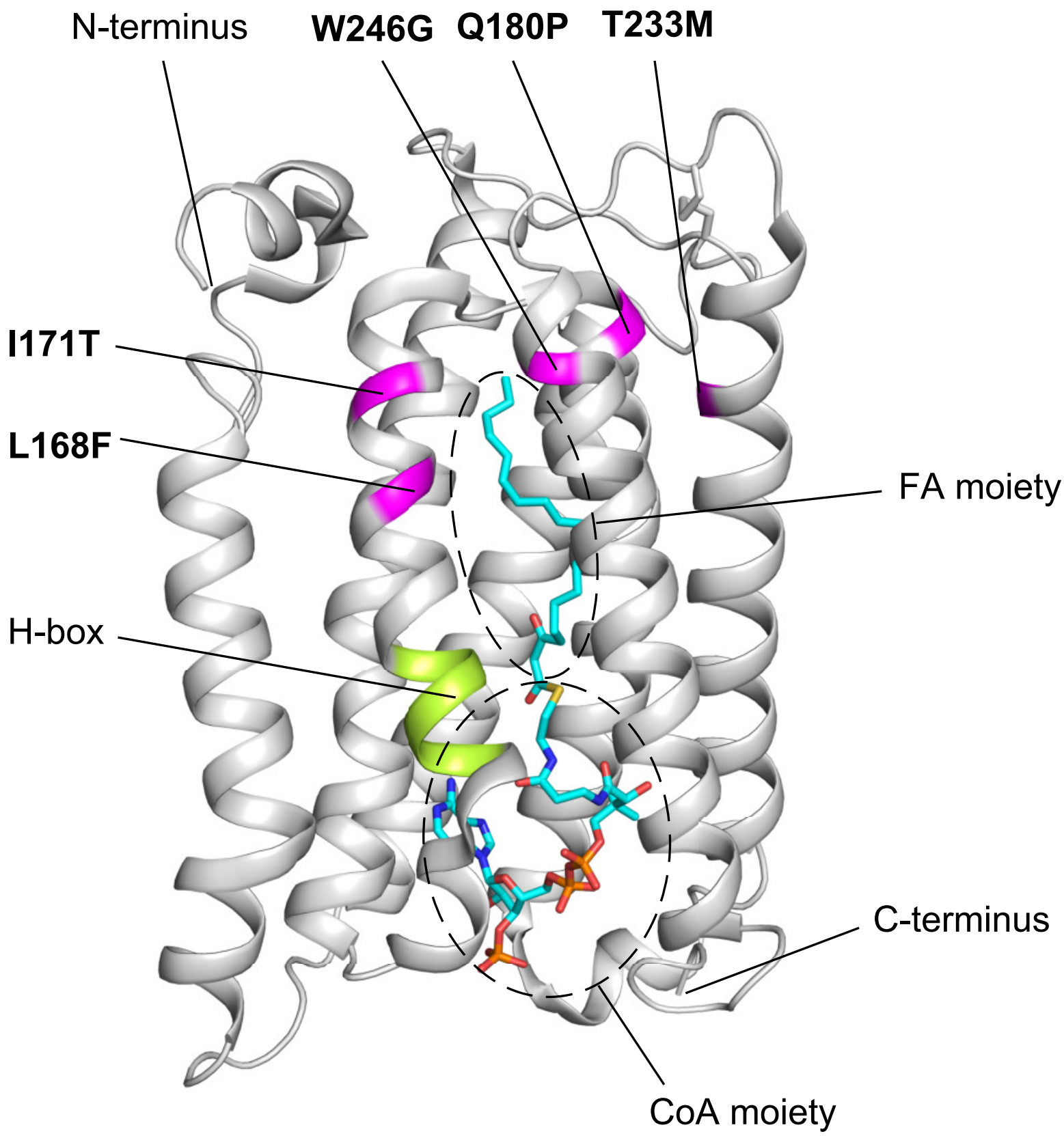


Fig. 3

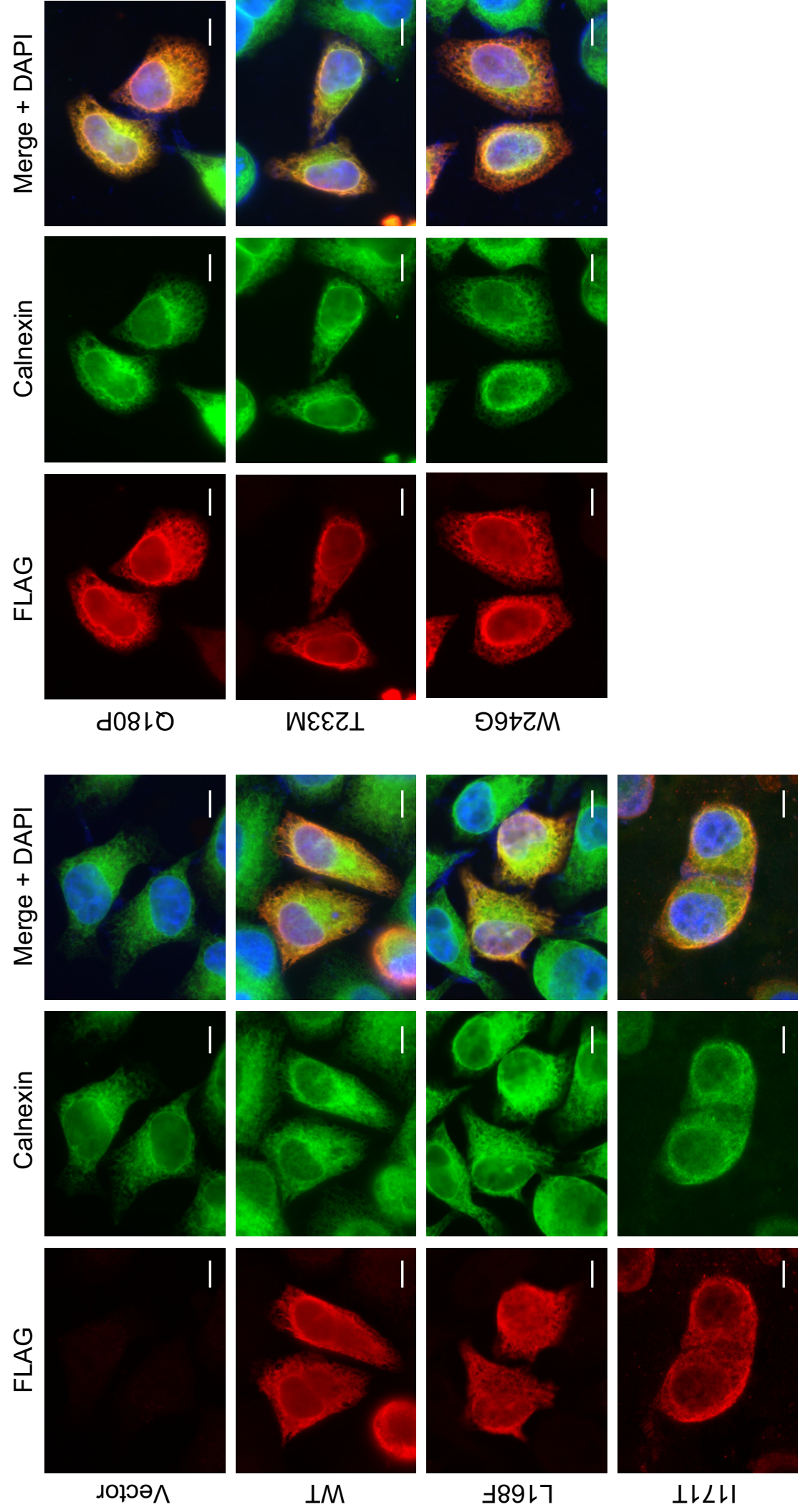


Fig. 4

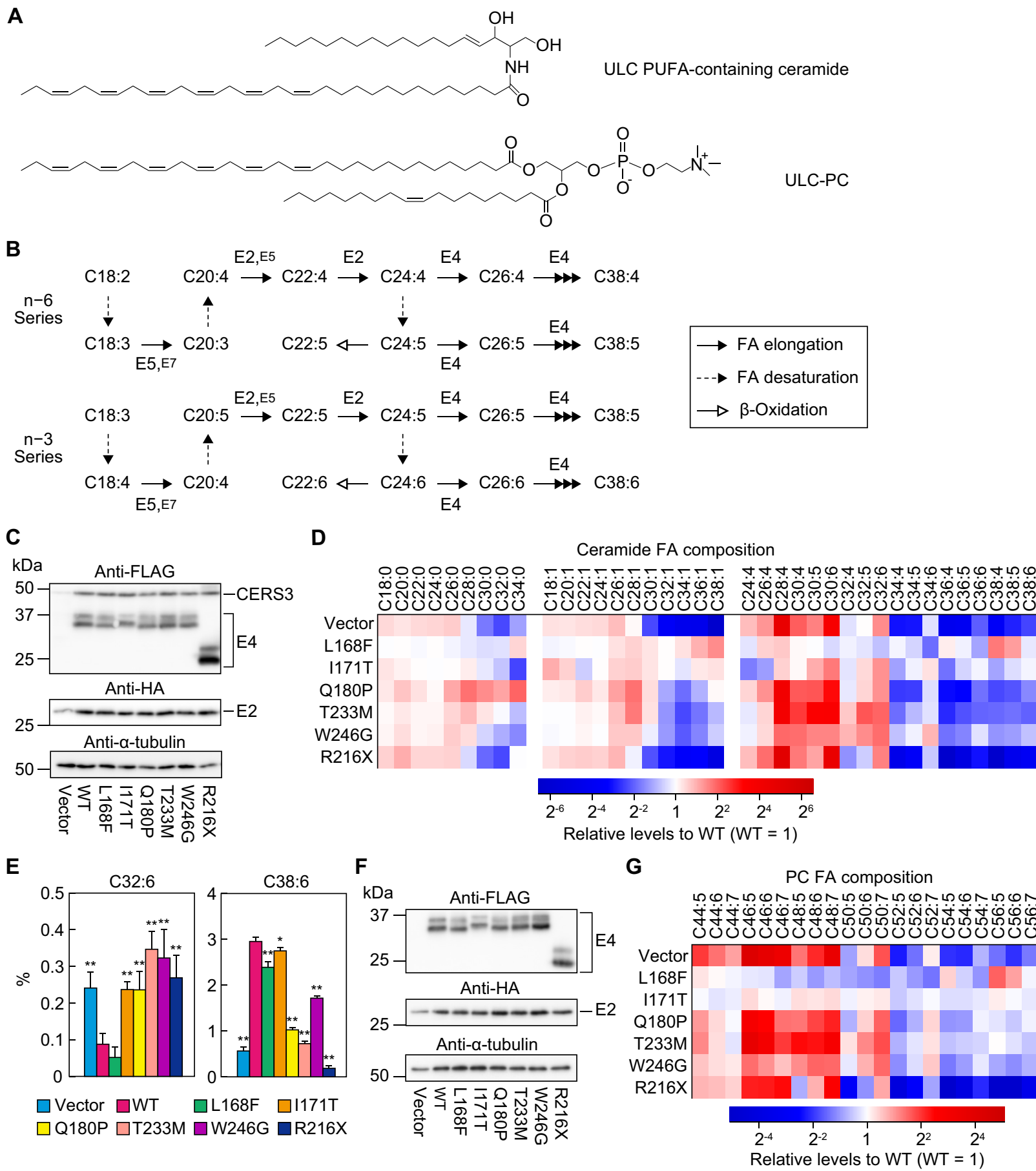


Fig. 5

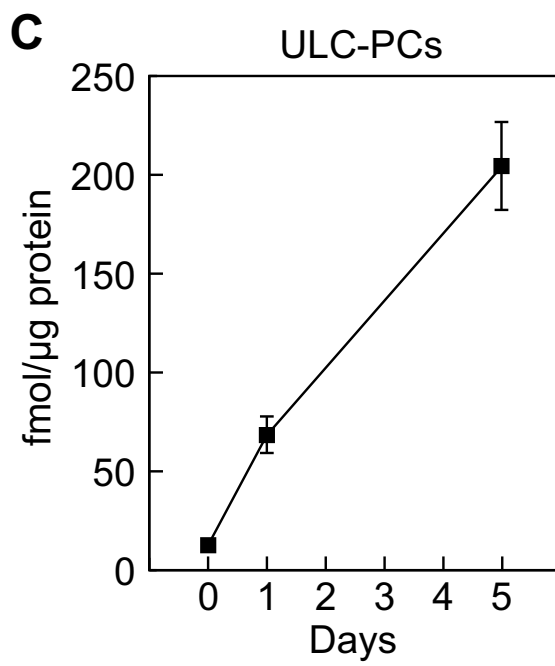
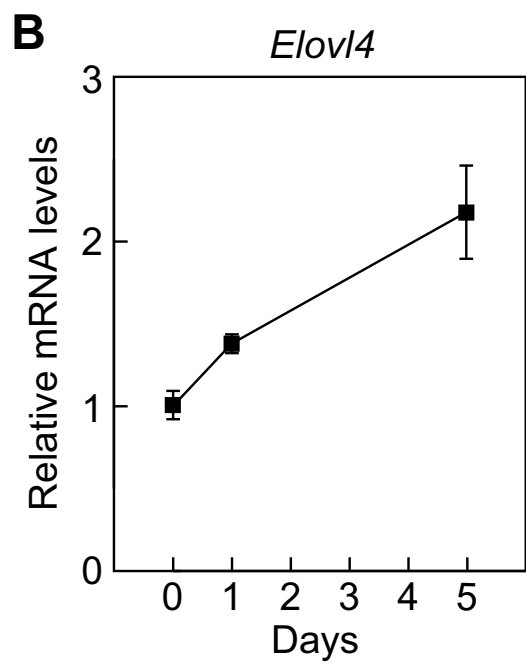
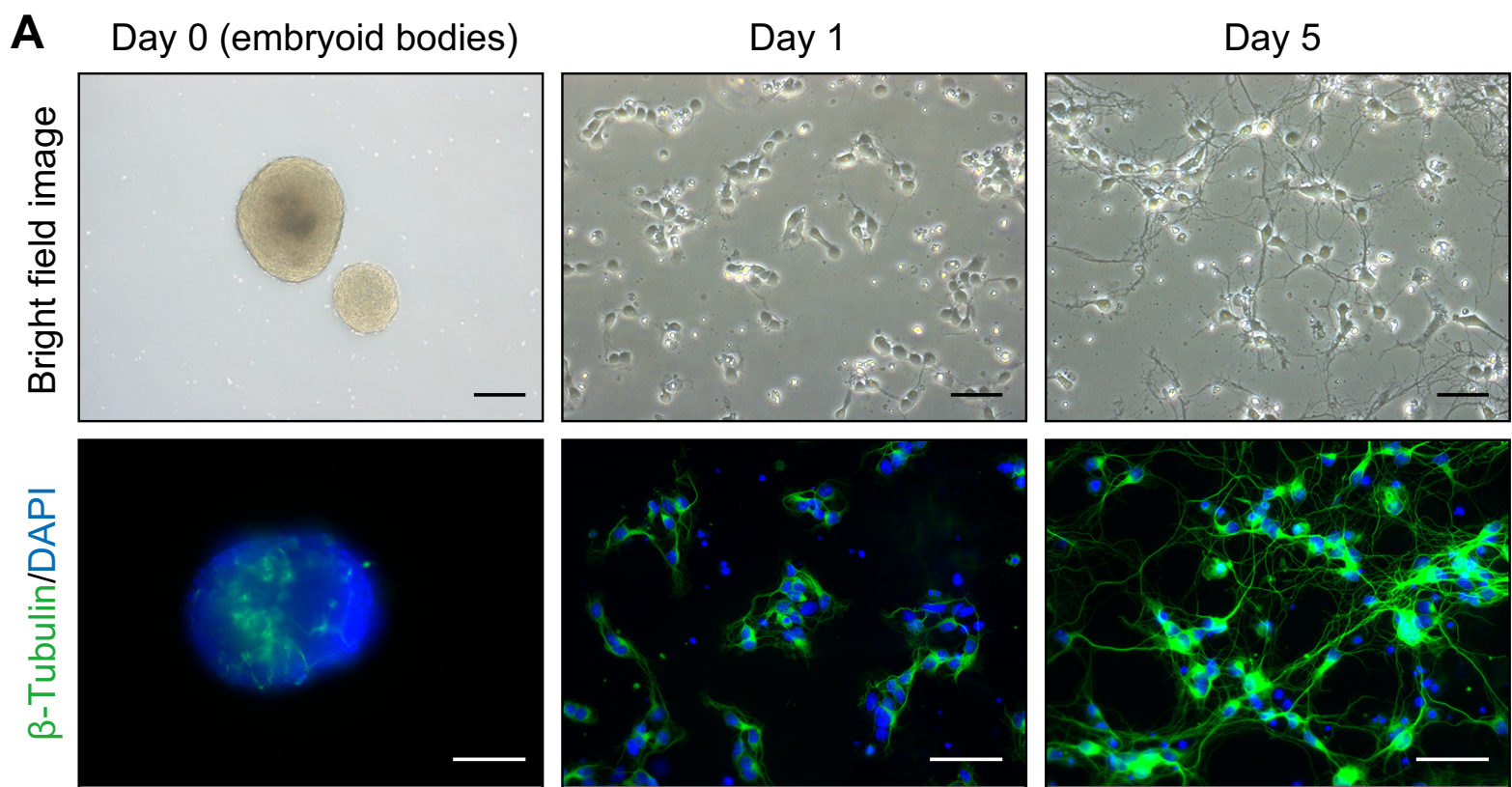


Fig. 6

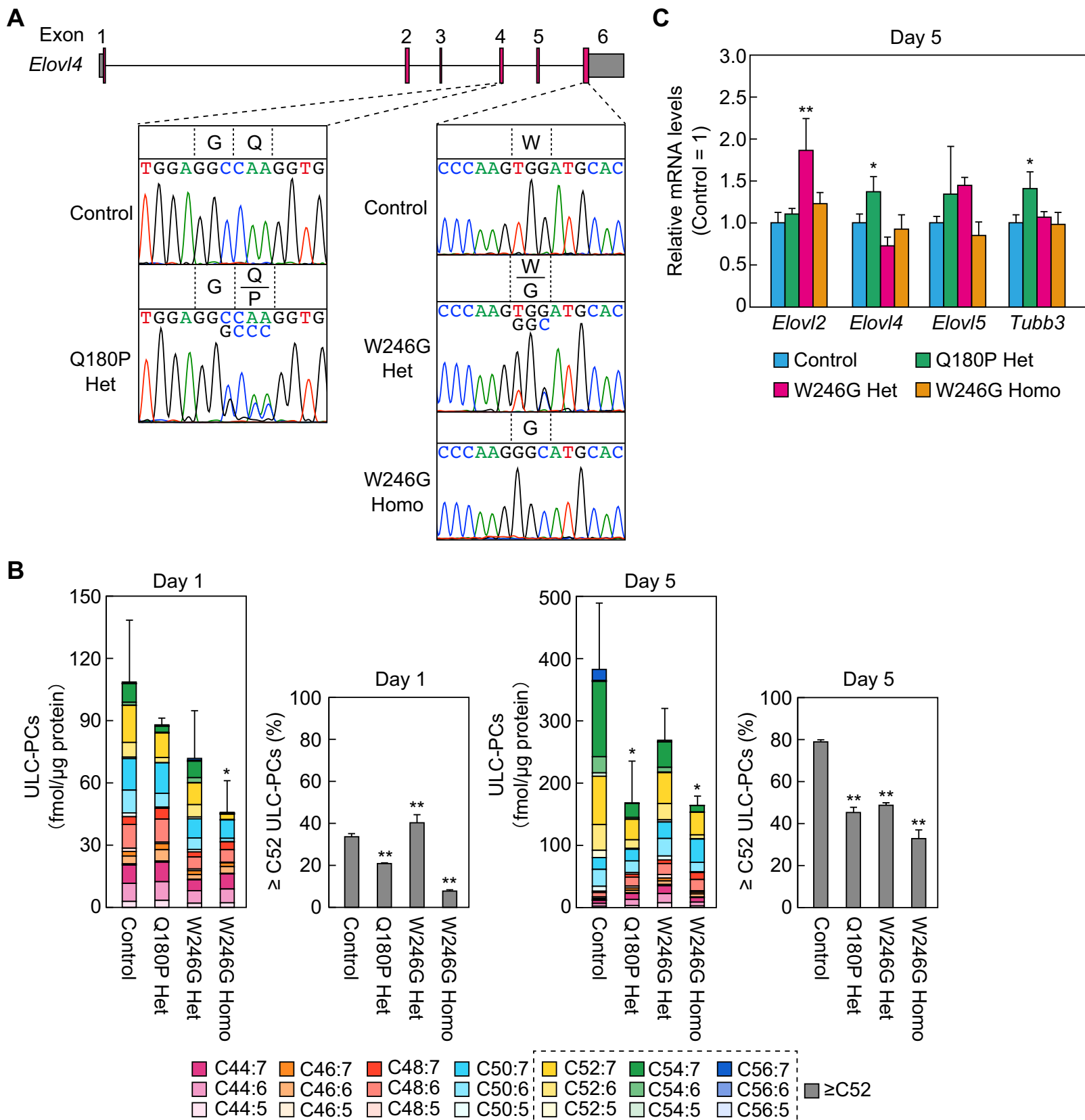


Fig. 7

